Weather systems in mid-latitudes

Chapter · January 2025

DOI: 10.1016/B978-0-443-15748-6.00005-8

7 authors, including:

Jennifer Louise Catto
University of Exeter
81 PUBLICATIONS **2,802** CITATIONS
SEE PROFILE

Edgar Dolores
University of Bern
11 PUBLICATIONS **51** CITATIONS
SEE PROFILE

Matthew Priestley
University of Exeter
30 PUBLICATIONS **800** CITATIONS
SEE PROFILE

Shira Raveh-Rubin
Weizmann Institute of Science
66 PUBLICATIONS **1,510** CITATIONS
SEE PROFILE

Weather systems in mid-latitudes

Duncan Ackerley[a], Jennifer L Catto[b], Edgar Dolores-Tesillos[c], Matthew DK Priestley[b], Shira Raveh-Rubin[d], Reinhard Schiemann[e], and Charlie C Suitters[b], [a]Met Office, Exeter, United Kingdom; [b]Department of Mathematics and Statistics, University of Exeter, Exeter, United Kingdom; [c]Institute of Geography, Oeschger Centre for Climate Change Research, University of Bern, Bern, Switzerland; [d]Department of Earth and Planetary Sciences, Sussman Family Building for Environmental Sciences, Weizmann Institute of Science, Rehovot, Israel; [e]Department of Meteorology, University of Reading, National Centre for Atmospheric Science (NCAS), Reading, United Kingdom

Abstract

This article describes the development and structure of the weather systems that traverse the mid-latitudes of both hemispheres. First, a review of how rotation and thermal gradients set the background state for weather system development is described. Second, a description of mid-latitude storm (extratropical cyclone) structure, development and their associated features (wind flows and fronts) are presented. Finally, the development and lifecycle of blocking anticyclones is discussed along with a discussion of how their impacts vary depending on the season in which they develop.

Keywords

Anticyclone; Baroclinic; Blocking; Conveyor belt; Extratropical cyclone; Front; Geostrophic; Jet stream; Norwegian model; Shapiro-Keyser model

Glossary

Adiabatic/diabatic Adiabatic processes are those which exchange neither mass nor energy with the surrounding environment. Conversely, diabatic processes are those which transfer mass or energy to or from the environment (e.g., air being heated by emission of terrestrial long-wave radiation).
Conditional symmetric instability An air parcel that is stable to vertical (static stability) and horizontal (inertial stability) displacement but is unstable to slantwise (i.e., simultaneous vertical and horizontal displacement) movement when it becomes saturated (latent heat release).
Potential instability A parcel is potentially unstable if, at the point of being lifted to saturation, becomes more buoyant than the surrounding air and accelerates upwards.
Potential temperature The temperature a parcel of air would have if it were compressed or decompressed adiabatically to a pressure of 1000 hPa.
Potential vorticity (PV) The scalar product of absolute vorticity and the gradient in potential temperature. It can only be changed through diabatic processes (e.g., latent heating) or friction and therefore is conserved by fluid parcels as they move with the flow.
Rossby wave A large-scale (planetary) wave that forms in a flow (typically in westerly flow in the mid-latitudes) on a rotating surface (e.g., Earth) and results from the conservation of potential vorticity on air parcels that are displaced from their reference position.
Tropopause fold The tropopause is the boundary between the troposphere and stratosphere and is identified by a large increase in static stability. A tropopause fold is where the boundary is deformed (folded) in the vicinity of an extratropical cyclone and stratospheric air extends towards the surface.

Key points

- What is an extratropical cyclone?
  - o A three-dimensional, circulating weather system found in the mid-latitudes of both hemispheres with relatively low pressure at its center.
  - o A system that develops due to the presence of a low-level thermal gradient and/or an upper-level jet stream.
  - o A system that has several development pathways depending on the atmospheric flow structure (e.g., Norwegian and Shaprio-Keyser).
  - o A system that typically contains thermal boundaries (fronts), which can be associated with hazardous weather.
  - o A type of system that may bring major social and economic hazards for societies within the mid-latitudes.
- What is an anticyclone/blocking anticyclone?
  - o A three-dimensional circulating system found in the mid-latitudes with relatively high pressure at its center.
  - o A weather feature that may become stationary or slow moving and block the eastward propagation of extratropical cyclones.
  - o A system that may bring prolonged dry spells, extreme heat (summer) or exceptional cold (winter) to the mid-latitude regions they persist over.

Introduction

Unlike in the tropics, where circulations respond more directly to surface heating from the sun, weather in the mid-latitudes is governed by both differential surface heating and the Earth's rotation on its axis. It is the rotation of the Earth that gives rise to the circular motions of the large-scale weather systems that traverse the mid-latitudes of both hemispheres. To give an example, a region of high pressure (denoted "H") and low pressure (denoted "L") are shown in Fig. 1. The purple arrow denotes the direction of the pressure gradient from high to low, which is the direction air would travel in the absence of rotation. Instead, the air is deflected to the right of the pressure gradient and turns clockwise around the high-pressure center and anticlockwise around the low-pressure center in the Northern Hemisphere (the opposite is true for the Southern Hemisphere). This deflection to the right is caused by the Coriolis effect (red, dashed arrow in Fig. 1), which depends on both the axial rotation of Earth's surface and the motion of the air relative to it. The balance between the pressure gradient force and Coriolis effect is known as geostrophic balance and the flow resulting from that balance (the geostrophic wind V_g, m s^{-1}) can be written as:

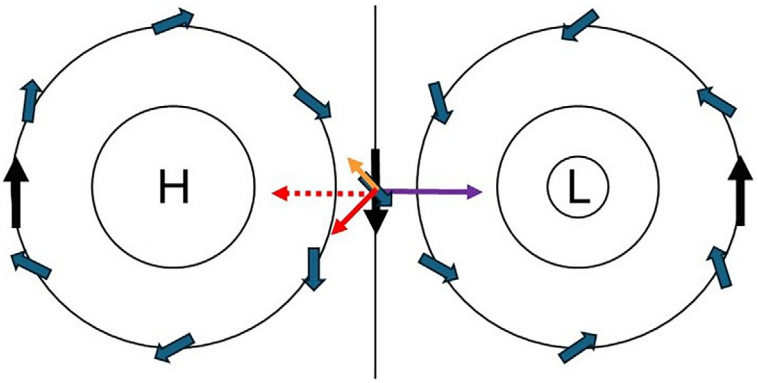

Fig. 1 Circulation and balances of forces around high (H) and low (L) pressure centers in the Northern Hemisphere. Black arrows are the idealized flow without friction, the purple arrow represents the pressure gradient force (from high to low), the red dashed arrow represents the action of the Coriolis effect perpendicular and to the right of the flow in a frictionless environment. The teal arrows are representative of the actual flow around the pressure centers, with friction (orange arrow) acting against the flow, which reduces the magnitude of the Coriolis effect near the Earth's surface (solid red arrow) and enables the flow to turn across the isobars in the configuration shown.

$$V_g = \frac{1}{\rho f}\frac{\partial p}{\partial n} \tag{1}$$

where ρ is the air density (kg m^{-3}), f is the Coriolis term (s^{-1}), ∂p is the difference in pressure between two points (Pa) and ∂n is the distance (m) between the two points under consideration and perpendicular to the flow. While geostrophic balance provides a close approximation to the observed large-scale atmospheric circulations, other effects such as the centripetal acceleration and friction prevent geostrophic balance from ever being achieved. For example, friction (orange arrow, Fig. 1) acts to slow the wind, which reduces the magnitude of the Coriolis effect (red, solid arrow in Fig. 1) and allows cross-isobaric drift to occur (teal arrows, Fig. 1). Without such a process, the pressure minimum would remain indefinitely, and mid-latitude weather systems would not decay, which is clearly unrealistic. Nevertheless, for large-scale synoptic motions the tendency towards geostrophic balance is very useful for explaining other processes important in mid-latitude weather.

Another relevant factor in the mid-latitudes is the presence of a large temperature gradient due to the differential heating of the tropics (warm) and the poles (cold). The gradient leads to pressure ("baro") surfaces being inclined ("clinic") relative to temperature surfaces, giving rise to what is known as a "baroclinic atmosphere." The zonal mean air temperatures (with pressure as the vertical co-ordinate) for January and July are plotted in Fig. 2a and b, respectively. The largest angle (inclination) between the isotherms (shading) and isobars (dotted horizontal lines) can be seen between approximately 30°N-60°N and 30°S-60°S, i.e., in the mid-latitudes and indicates a region of large "baroclinicity." There is also a clear seasonal cycle to the baroclinicity, which is larger in the mid-latitudes of the winter hemisphere. Overlaid (yellow lines) in both Fig. 2a and b are the zonal mean geopotential heights of

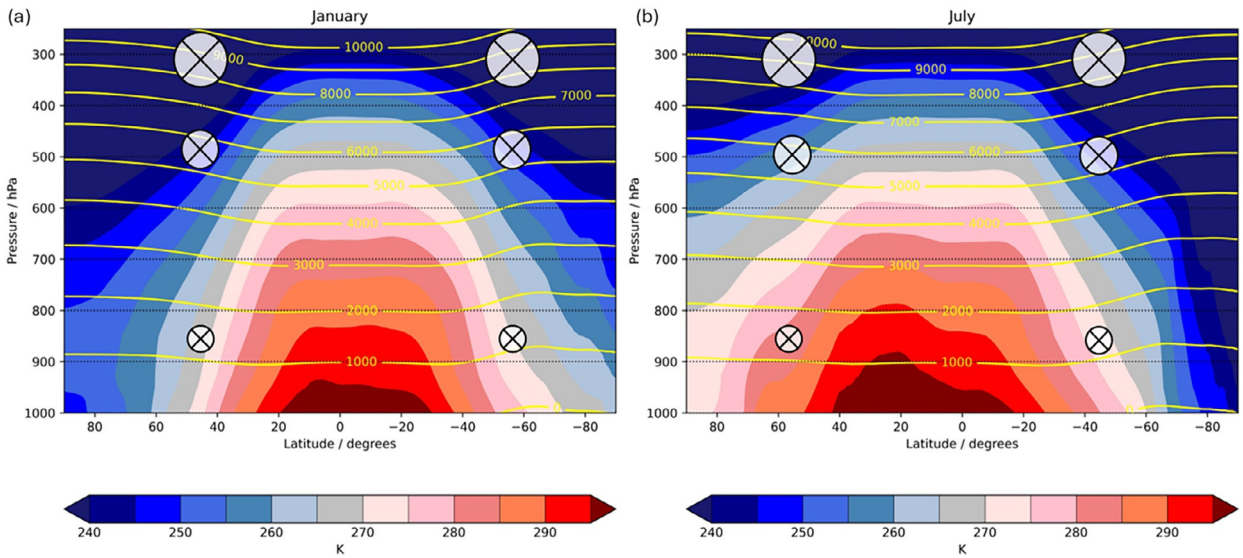

Fig. 2 Zonal mean temperature (K, shaded) and geopotential height (m, yellow contours) on pressure levels for (a) January and (b) July from ERA5 (Hersbach et al., 2023) averaged over 1980–2022. Approximate locations of wind maxima at 950 hPa, 500, and 300 hPa are indicated by the crosshairs.

atmospheric pressure levels. The heights can be interpreted as the height of the pressure surfaces above mean sea level (Zp), which can then, in combination with hydrostatic balance,[1] be used to re-write the geostrophic wind equation as:

$$V_g = \frac{g}{f}\frac{\partial Z_p}{\partial n} \tag{2}$$

where g is the acceleration due to gravity (9.81 m s^{-2} on Earth) and ∂Z_p is the difference in pressure level geopotential height (m) over distance ∂n (m). From Fig. 2a and b there is a latitudinal gradient in the geopotential height contours in the mid-latitudes–particularly in the winter hemisphere. Moreover, in both hemispheres, the difference in vertical height of a specific pressure level between 30° and 60° latitude increases with height, which is displayed in Table 1. Therefore, from Eq. (2) and Table 1 the upper-level isobaric geostrophic wind would be larger than the isobaric geostrophic wind near the surface. Therefore, in regions of high baroclinicity, a band of strong winds at upper levels occurs, which is also known as a jet stream.

Such jet streams are not a continuous feature across the hemisphere and are not equal in length or strength. They appear intermittently where there are strong, local temperature gradients, and therefore have "entrance" and "exit" regions where the flow is accelerated and decelerated, respectively (depicted in Fig. 3). For geostrophic balance to be maintained, the pressure gradient and Coriolis terms must be equal and opposite in magnitude leading to a steady state where no acceleration of the flow occurs, which cannot be true at the jet entrance and exit regions. Moreover, if there is a perpetual steady state then the flow would not evolve and no weather systems could develop, which is unphysical. To understand one way the upper-level jet may relate to surface weather system development, a flow known as the ageostrophic wind (V_a, m s^{-1}) is introduced and is simply the difference between the actual wind (V, m s^{-1}) and the geostrophic wind (V_g, m s^{-1}):

$$V_a = V - V_g \tag{3}$$

The capitalized V has both zonal (west-to-east) and meridional (equator to pole) components. If we take the zonal component of Eq. (1) and introduce an acceleration term, the resulting expression can be written as:

Table 1 The mean difference (between 30° and 60° latitude) in the geopotential height (m) of pressure levels (950, 500, and 300 hPa) for each hemisphere averaged over 1980–2022 from ERA5 in January and July.

30–60° ΔZ_p (m)	*Northern hemisphere*			*Southern hemisphere*		
	950 hPa	*500 hPa*	*300 hPa*	*950 hPa*	*500 hPa*	*300 hPa*
January	113	491	753	256	618	869
July	49	261	432	294	624	885

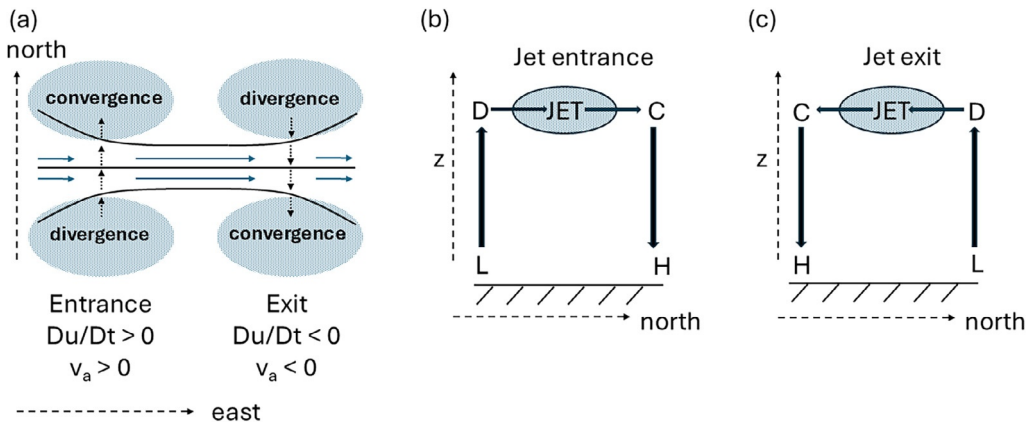

Fig. 3 Schematic diagram of the characteristic flow patterns around the entrance and exit to a jet stream. (a) Plan view (north and east indicated) of a jet stream entrance and exit indicated by the streamlines converging and diverging (solid lines) and flow strength indicated by the length of the blue arrows. Overlaid with the dashed arrows are the northward (southward) ageostrophic flow across the jet stream entrance (exit). Regions of divergence and convergence are indicated and labelled. (b) Vertical cross section through the jet (labeled) entrance showing the upper-level divergence (D) and convergence (C) regions and the induced vertical motion leading to lower (L) or higher (H) pressure at low-levels. (c) The same as (b) except for the jet stream exit region. Figures (b) and (c) align with the dashed arrows in (a) with the jet flowing out of the page towards the reader.

[1] $dp/dz = -\rho g$ where dp/dz is the vertical pressure gradient (Pa m^{-1}), ρ is the air density (kg m^{-3}) and g is the acceleration due to gravity (m s^{-2}).

$$\frac{Du}{Dt} = fv - \frac{1}{\rho}\frac{\partial p}{\partial x} \tag{4}$$

where Du/Dt is the acceleration of the zonal wind (m s^{-2}), f is the Coriolis term (s^{-1}), ρ is the air density (kg m^{-3}), v is the meridional wind speed (m s^{-1}), ∂p/dx is the pressure gradient in the east-west direction between two points under consideration (Pa m^{-1}). *Re*-arranging Eq. (4) and substituting in for the meridional component of the wind (v) from Eq. (3) results in:

$$\frac{Du}{Dt} = fv_a + fv_g - \frac{1}{\rho}\frac{\partial p}{\partial x} \tag{5}$$

From Eq. (1), the expression for the meridional component of the geostrophic wind would be:

$$v_g = \frac{1}{\rho f}\frac{\partial p}{\partial x} \tag{6}$$

Substituting Eq. (6) into Eq. (5) results in the cancellation of the second and third terms of Eq. (5), which results in the acceleration of the zonal wind being proportional to the meridional component of the ageostrophic wind given in Eq. (7) (i.e., at right angles to the acceleration).

$$\frac{Du}{Dt} = fv_a \tag{7}$$

Thus, in the Northern Hemisphere (Fig. 3a), acceleration (Du/Dt > 0) of the upper-level flow results a northward ageostrophic flow ($v_a > 0$), which induces divergence to the right of the jet entrance, and therefore low-level ascent and a reduction in surface pressure (denoted by the "L" in Fig. 3b). Similarly, deceleration (Du/Dt < 0) of the upper-level flow results in a southward ageostrophic flow ($v_a < 0$) with divergence induced to the left of the jet exit (in the Northern Hemisphere). Thus, the divergence region to the left of the jet exit is also associated with low-level ascent and a reduction in surface pressure (denoted by the "L" in Fig. 3c). Therefore, in the Northern Hemisphere the "right jet entrance" and "left jet exit" regions are conducive to development and/or deepening of low-pressure weather systems because of the forced ascent. The opposite is true in the Southern Hemisphere with the left jet entrance and right jet exit regions favorable for development.

Given the descriptions above, the combination of the Earth's rotation, the presence of a strong temperature gradient and an upper-level jet stream often lead to the highly varied and interesting weather features of the mid-latitudes described below.

Extratropical cyclones

What is a cyclone?

From the schematic in Fig. 1, a cyclone is a region of inward circulating air directed towards a minimum in atmospheric pressure. The air in a cyclone rotates anticlockwise in the Northern Hemisphere and clockwise in the Southern Hemisphere. While the basic anatomy of a cyclone is relatively easy to describe, the development, three-dimensional structure and decay of such features is considerably more complex. Therefore, it is sensible to begin with the early concepts of extratropical cyclones (concepts that are relevant now and still taught in schools and universities today) followed by a deeper exploration of the weather features associated with them and their development.

Early concepts: The Norwegian model

Structure of the mature cyclone

The most well-known conceptual model, and the first to be generally accepted, was the Norwegian Cyclone Model of extratropical cyclones introduced by Jacob Bjerkness at the Bergen School of Meteorology in Norway (Bjerknes, 1919). The final, and most well-known iteration of the Norwegian Model is presented in "plan view" in Fig. 4(ii) and is adapted from Bjerknes and Solberg (1922). The cyclone is propagating from left to right in the figure (indicated by the dot-dashed arrow) and the center of the cyclone is denoted by a yellow cross. There is a clear asymmetrical structure to the cyclone, with a wedge of warm air in the southern portion of the cyclone (denoted the warm sector) surrounded by cold air (now known as the cold sector). The cyclonic (anticlockwise) flow of the wind is indicated by the solid arrows with filled arrows for the cold air flow and unfilled arrows for flow within the warm sector. The boundaries between the warm sector and cold air are denoted as the warm (red line and scallops) and cold (blue line and triangles) fronts, with the warm front at the leading edge of the warm sector and the cold front at the back edge (or leading edge of the cold sector). The hatched area ahead of the warm front, behind the cold front and to the north of the cyclone center indicates regions of cloud and precipitation. The cloud and precipitation are associated with forced ascent of lower density (warmer) air over higher density (colder) air, which is described in more detail in the Fronts section, below.

There are also two cross sections of the cyclone denoted in Fig. 4(ii), which are denoted as AB to the north of the cyclone center and CD to the south. The cross sections display the representative weather and cloud features that an observer at either point might encounter. The sequence of events is familiar to many in the mid-latitudes along both cross sections as the cyclone passes overhead. The CD observer, starting in the cold sector ahead of the warm front, notices the development of high cirrus clouds overhead at the leading edge of the warm sector high in the troposphere (denoted as ca. 9 km in Fig. 4(iii)). As the upper-level warm sector

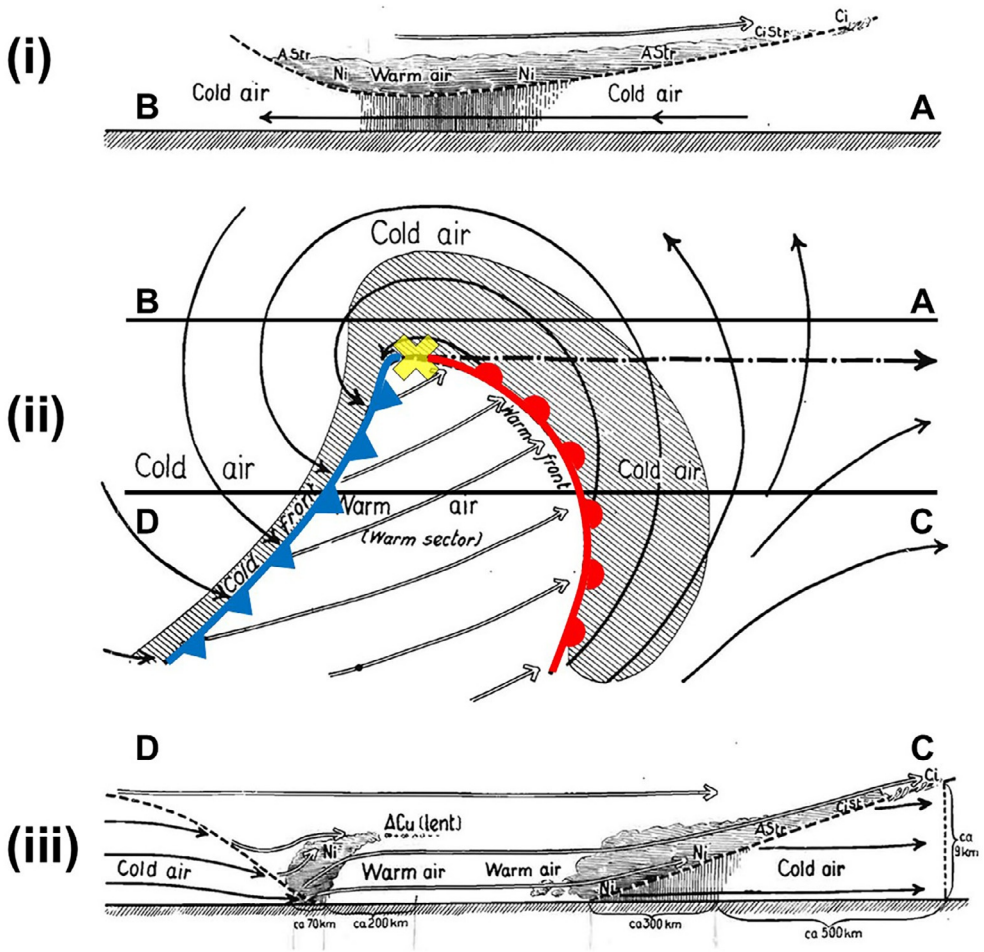

Fig. 4 The structure of an idealized cyclone, which became known as the "Norwegian cyclone model." (i) upper (unfilled arrow) and lower (filled arrow) air flows and the cloud structure encountered by an observer along points A to B (as denoted in (ii)), (ii) air flow (solid and unfilled arrows), direction of propagation (dot-dashed arrow), cyclone center (yellow cross), warm front (red line and scallops), cold front (blue line and triangles), (iii) as in (ii) except for an observer along points C to D (as denoted in (ii)). Adapted and reproduced with permission from Bjerknes J and Solberg H (1922) Life cycle of cyclones and the polar front theory of atmospheric circulation. *Geophysica Norvegica* 3(1): 3–18. https://geofysikk.org/NGF/GeoPub/NGF_GP_Vol03_no1.pdf.

boundary descends, the cloud deepens into cirrostratus and then altostratus where precipitation may start to reach the ground ahead of the surface front. Further deepening of the cloud into nimbostratus and heavier precipitation follows next before the surface warm front passes. The passage of the warm front is then associated with a veering of the wind (from southeasterly to southwesterly in the Northern Hemisphere), an increase in air temperature and a reduction in cloud cover. Typical weather in the warm sector would be broken stratocumulus cloud and light precipitation. The observer would then encounter the rain band associated with the cold front, which tends to be narrower with heavier precipitation falling from cumulus-congestus or cumulonimbus cloud. As the surface cold front passes, the person would note another veering of the wind (from southwesterly to northwesterly in the Northern Hemisphere) and drop in air temperature as they transition into the cold sector behind the front.

Ultimately, what Bjerknes and others at the Bergen School recognized was that the weather (i.e., cloud and precipitation) are tied to regions of forced ascent within the cyclone and do not occur randomly throughout. A clear structure could be seen, along with important cloud and precipitation features, and therefore a forecast could be made if you knew where you were within the system and the speed and direction of propagation. Bjerknes also noted the different view of an observer to the north of the cyclone center (denoted AB in Fig. 4(i)) who would not encounter the warm sector air at the surface but still experience the passage of a region of cloud and precipitation. The sequence of events observed between AB show a clear vertical structure to the cyclone, which varies depending on where an observer is placed.

Lifecycle

While the previous sections describe the main features of the Norwegian Model for mature extratropical cyclones, the Bergen School meteorologists recognized there was a clear evolutionary pathway, or "lifecycle," to these systems. The typical lifecycle of a cyclone from the Norwegian Model is depicted in four main stages in Fig. 5a. An incipient cyclone (denoted by "I" in Fig. 5a) forms along a

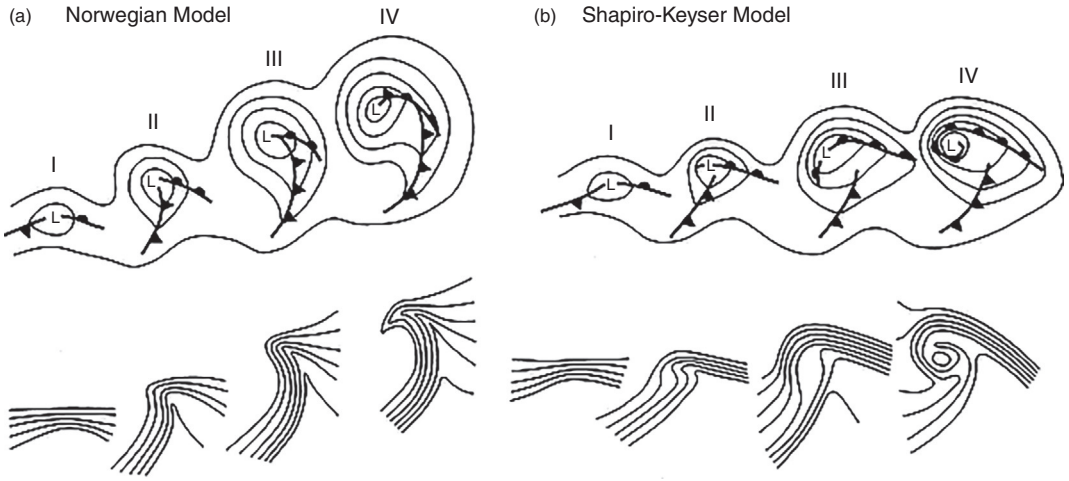

Fig. 5 Development stages for (a) Norwegian and (b) Shapiro-Keyser cyclones. Top row depicts geopotential heights (minima indicated by the "L") and fronts, and isotherms (potential temperature) are displayed in the bottom row with both rows representative of lower-tropospheric (ca. 850 hPa) conditions. For (a), (I) is the insipient cyclone formation on a frontal zone, (II) narrowing of the warm sector that continues into (III) with the occluding cyclone in (IV). For (b), (I) is again the insipient frontal cyclone, frontal fracturing occurs in (II), the development of the bent back front and T-bone structure in (III), and finally the warm seclusion becoming apparent in (IV). The times between stages are approximately 6–24 h. Length scales are approximately 1000 km from the "L" to the outermost height contour in the stage (IV) figures. From Fig. 15 in Schultz DM, Keyser D, and Bosart LF (1998) The effect of large-scale flow on low-level frontal structure and evolution in midlatitude cyclones. *Monthly Weather Review* 126: 1767–91. https://doi.org/10.1175/1520-0493(1998)126<1767:TEOLSF>2.0.CO;2. © American Meteorological Society. Used with permission.

strong thermal gradient (i.e., a front, see the Fronts section, below). As the cyclone deepens (denoted "II" in Fig. 5a), the thermal gradient along the cold front strengthens and extends meridionally, whereas the temperature gradient of the warm front becomes less pronounced. As the cyclone reaches maturity (denoted "III" in Fig. 5a and equivalent to Fig. 4(ii)) the strong thermal gradient across the cold front is maintained and rotates around the cyclone towards the warm front causing the warm sector to narrow. Finally, (denoted 'IV' in Fig. 5a) the cyclone occludes (and decays) with the cold front either ascending over (warm occlusion) or lifting (cold occlusion) the cold sector air to the east (more detail in the Occluded fronts section). Therefore, an extratropical cyclone acts to remove the initial horizontal thermal gradient as the warm sector is lifted above the cold sector. The rearrangement results in a reduction of potential energy as the warmer (less dense) air now lies above the cooler (denser) air with little trace of the original surface thermal gradient (occluded front).

While the conceptual model developed by the Bergen School described many of the events typically associated with mid-latitude cyclones, it became clear that the Norwegian Model of cyclone development did not fit all observed cyclones as the observational network grew. Other models have been developed since that early work to account for the broad family of development mechanisms and structural components of extratropical cyclones, which are discussed below.

Expansion of understanding

The Shapiro-Keyser model

By the end of the 1980s, it was becoming clear that the Norwegian Model of extratropical cyclone lifecycles did not fit all cases, and a separate conceptual model might be required. While the systems observed by the Bergen Meteorologists developed in a mixture of marine and terrestrial environments over Europe, there was growing evidence that extratropical cyclones developing in an entirely marine environment might differ from the "incipient wave—frontal cyclone—occlusion" lifecycle of the Norwegian Model. Shapiro and Keyser (1990) noted fracturing of the cold front, the wrapping of the warm front, a seclusion of warm air and a lack of an occluded front all in proximity to the cyclone center, were common features in several idealized modelling studies. However, due to the idealized nature of those modelling studies described by Shapiro and Keyser (1990), none of these features could be associated with real-world extratropical cyclones. What Shapiro and Keyser (1990) then did was to consult observational evidence to support the modelling studies and showed that the features simulated by the models did (and do!) occur in the real world. They were then able to produce a new, and complimentary, conceptual model of the lifecycle of extratropical cyclones depicted in Fig. 5b.

The incipient cyclone (denoted "I" in Fig. 5b) forms in a baroclinic zone that resembles the same stage in the Norwegian Model. As the cyclone develops, frontal fracture occurs near the cyclone center (denoted by "II" in Fig. 5b) with stronger baroclinicity on the warm front than the cold front. Next, the separation between the warm and cold fronts increases resembling a "T-bone" shape (denoted "III" in Fig. 5b) with the warm front (and its strong baroclinicity) bending back poleward and westward of the cyclone center. Finally, cold air encircles the region of relatively warmer air in the center of the cyclone leading to the development of a

warm-core seclusion (denoted 'IV' in Fig. 5b). The Shapiro-Keyser cyclones also tend to be more "zonally elongated" whereas their Norwegian counterparts are more "meridionally elongated," which is also depicted in Fig. 5a and b. It is also worth noting that Shapiro and Keyser (1990) named this type of cyclone a "marine cyclone" rather than a "Shapiro-Keyser" cyclone, as they are known today. It has since been found that such cyclones are not restricted to marine areas and the development of both "Shapiro-Keyser" and "Norwegian" cyclones depends on the vertical structure of the environment in which they form.

The influence of the jet stream on development

As described in the introduction, the role of a jet stream and its structure are important for the development of extratropical cyclones. Moreover, the location of surface cyclone development relative to a jet stream can set the conditions responsible for a cyclone following the Shapiro-Keyser or Norwegian lifecycle models.

In the mid-latitudes, a jet stream is a ribbon of very strong winds located high above the surface of the Earth travelling from west to east (westerly). The strongest wind is typically located in the center of the ribbon (i.e., the jet core) with the wind decreasing uniformly either side of the jet core, as shown in Fig. 3a. Such a jet structure would be "unsheared" in the horizontal, i.e., the decrease in the flow either side of the jet center is symmetrical. In the real world however, the jets are rarely symmetrical about their cores. For example, the flow may decrease more rapidly poleward ("cyclonic shear") or equatorward ("anticyclonic shear") of the jet core. Such shearing is known as "across-jet" shear (i.e., perpendicular to the flow direction). The acceleration and deceleration of the flow in the jet entrance and exit regions, respectively (Fig. 3a) leads to "along-jet" shear (i.e., parallel to the flow direction). As the jet stream commonly forces cyclone development, the presence of shear (or not) within the upper-level jet stream ultimately leads to cyclones growing, maturing and decaying in different ways, i.e., they have different lifecycles. Cyclones that develop in each of the across-jet shear environments are described by Shapiro et al. (1999, and references therein) to be:

1. Life Cycle 1 (LC1) if they develop in the unsheared environment.
2. Life Cycle 2 (LC2) if they develop in the cyclonic shear environment.
3. Life Cycle 3 (LC3) if they develop in the anticyclonic shear environment.

Conversely, for development in the along-jet shear environments, Schultz and Zhang (2007) define the following:

1. CONF for cyclone development in the confluent (entrance) region of the jet.
2. DIFF for cyclones developing in the diffluent (exit) region of the jet.

In idealized modelling studies, extratropical cyclones developing in the LC1 environment are characterized by having a "T-bone" frontal structure with strong baroclinicity encircling the low-pressure center resulting in a warm seclusion, which conforms with the Shapiro-Keyser paradigm (Shapiro et al., 1999, and references therein). There is also strong evidence that confluence in the jet entrance regions acts to stretch cyclones in the zonal direction, resulting in strong baroclinicity along the warm front, which is a characteristic of Shapiro-Keyser cyclones (Schultz and Zhang, 2007). It therefore appears that Shapiro-Keyser cyclones tend to develop under the LC1 or CONF jet environments. Conversely, for idealized simulations with a cyclonically sheared environment (LC2), extratropical cyclones tend to develop an occluding warm sector with no frontal fracture, characteristic of the Norwegian Model (Shapiro et al., 1999, and references therein). Furthermore, simulated diffluence in the jet exit region tends to stretch cyclones meridionally with stronger baroclinicity along the cold front, which is also consistent with the Norwegian paradigm (Schultz and Zhang, 2007). Norwegian cyclones therefore tend to develop under a cyclonically sheared (LC2) or diffluent (DIFF) region of the jet. Finally, under anticyclonic shear, idealized cyclones tend to develop an "open wave" structure with a short warm front and a north-east to south-west orientated cold front. These open wave cyclones have no frontal occlusion and do not undergo a strong deepening phase. In summary, unsheared or confluent jet environments tend to lead to Shapiro-Keyser-type development and cyclonically sheared or diffluent jet environments lead to Norwegian-type cyclones.

Climatological distribution

Having identified the important structures and lifecycles of extratropical cyclones, it is important to discuss where they typically form, where they go and how intense they get. Fig. 6a–d show the seasonal mean track density (black contours), genesis density (yellow hatching) and mean intensity (shading) of extratropical cyclones in the Northern Hemisphere. Equivalent figures for the Southern Hemisphere can be found in Fig. 7a–d. Preferred genesis (formation) locations are in the lee of high topography (e.g., the Rocky Mountains and Himalaya in the Northern Hemisphere, and the Andes in the Southern Hemisphere), and over the ocean (e.g., North Atlantic, North Pacific and Southern Ocean). The cyclones then typically propagate eastwards in the prevailing westerly flow, increasing in intensity before decaying. The highest densities of extratropical cyclone tracks are generally found over the oceans of both hemispheres, along with the highest mean intensities. These favored regions of formation and propagation coincide with the largest low-level atmospheric temperature gradients (i.e., poleward of 40° latitude as can also be seen in Fig. 2).

There are clear seasonal variations in formation, propagation and intensity in both hemispheres, however. The highest track densities and mean cyclone intensities are found in the winter for both hemispheres (Figs. 6a and 7c), which is also when the number of extratropical cyclones forming is at its highest (large regions of yellow hatching), which corresponds with the largest temperature gradients across the mid-latitudes (Fig. 2). Conversely, the track densities and mean intensities of extratropical cyclones are at their lowest in the summer for both hemispheres (Figs. 6c and 7a) when the formation rates are also at their lowest

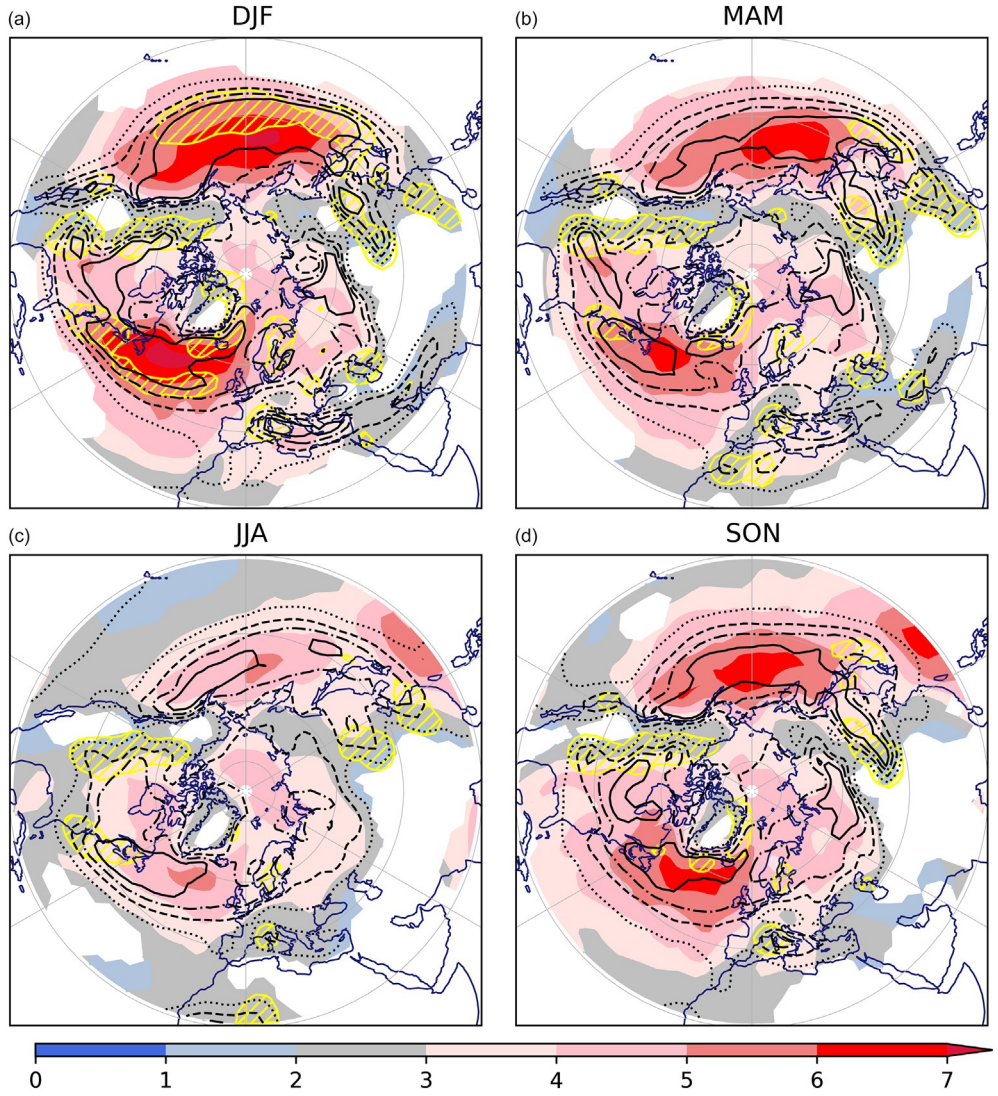

Fig. 6 Mean cyclone track density (contours, dotted at 3, dashed at 6, dot-dashed at 9 and solid at 12), genesis density (yellow hatching for greater than 1.2) and cyclone intensity (shading, s^{-1}) from ERA5 (1980–2022) in the Northern Hemisphere for positive vorticity features identified in the 850 hPa wind field using TRACK (see Hoskins and Hodges, 2019, and references therein). (a) December-January-February (DJF), (b) March-April-May (MAM), (c) June-July-August (JJA) and (d) September-October-November (SON). For track and genesis density, the units are number per month per 5° spherical cap. Mean intensity shading has been masked out where track densities are less than 1 (as done in Hoskins and Hodges, 2019). Map lines delineate study areas and do not necessarily depict accepted national boundaries.

(yellow hatching), which corresponds with the smallest temperature gradients across the mid-latitudes (Fig. 2). The highest track densities extend to lower latitudes in the winter and are restricted to higher latitudes in summer (especially over the ocean). There is also a clear tendency for extratropical cyclones to form in the lee of the Alps and track over the Mediterranean into Asia, particularly in DJF and MAM (Fig. 6a and b).

In the equinoctial seasons, there is a decrease extratropical cyclone formation and mean intensity for the spring relative to winter (Figs. 6b and 7d) and an increase for the autumn relative to the summer (Figs. 6d and 7b) in both hemispheres. There are also differences in the preferred cyclogenesis regions for spring relative to the autumn in both hemispheres. For the Northern Hemisphere, there are two clear favorable areas for cyclogenesis in spring over China and adjacent to the east coast of North America, which are less favorable in the autumn (compare Fig. 6b and d). In the Southern Hemisphere there are regions of cyclogenesis over Western Australia and the Tasman Sea in spring that are not visible during the autumn (compare Fig. 7d and b). Overall, extratropical cyclone activity is highest in the winter months and lowest in the summer months with a decrease (increase) in activity moving into spring (autumn) from winter (summer).

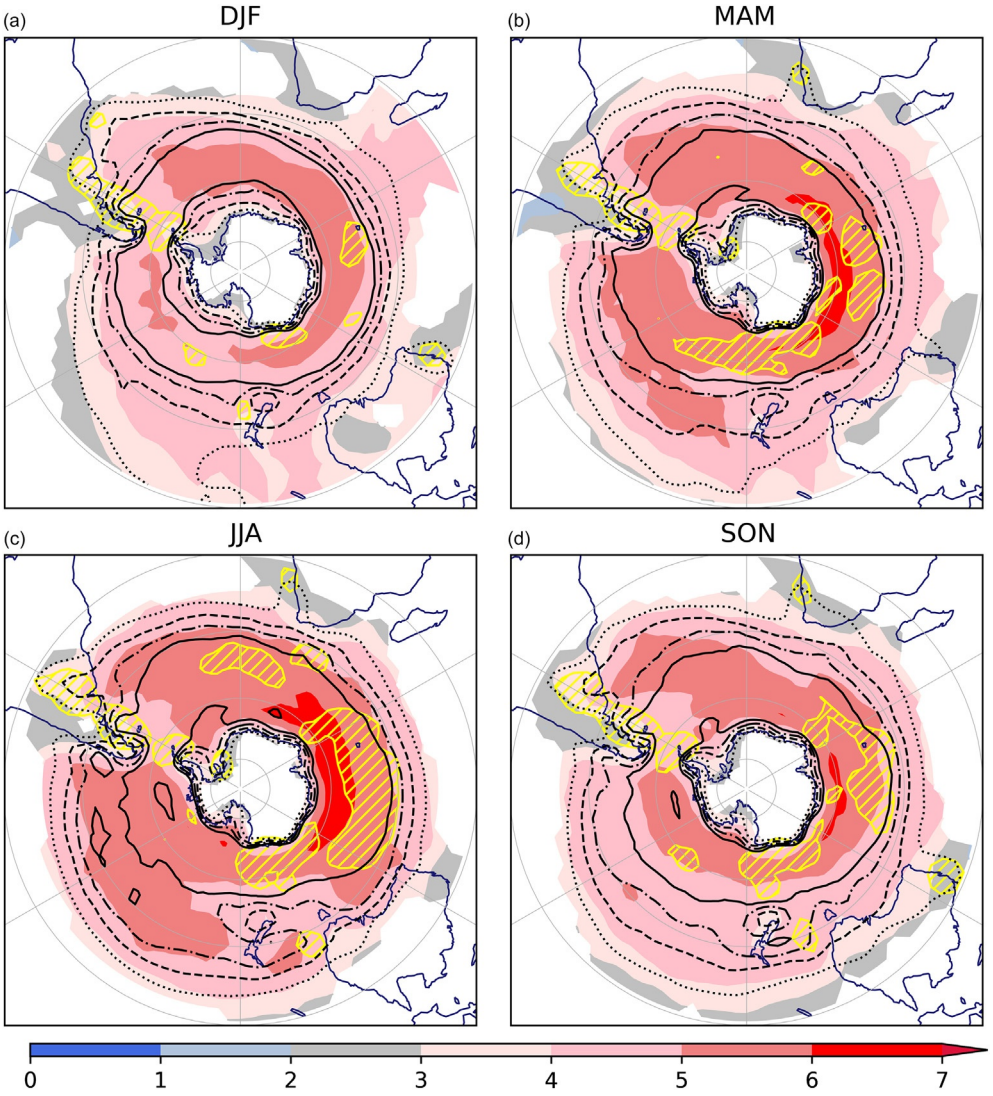

Fig. 7 The same as Fig. 6 except for the Southern Hemisphere. Map lines delineate study areas and do not necessarily depict accepted national boundaries.

Other cyclogenesis types

Explosive cyclogenesis

Occasionally, extratropical cyclones undergo rapid intensification with these commonly being known as "bomb cyclones." These cyclones are classified as distinct through their change in mean sea level pressure (MSLP) during their development and intensification phase. The key criteria, as set out by Sanders and Gyakum (1980), is for the mean sea level pressure to decrease by 24 hPa in 24 h (with latitudinal adjustment). The western boundaries of ocean basins are favorable environments for bomb cyclones due to the high moisture availability and strong temperature gradients commonly found there. These factors aid rapid intensification through baroclinic instability and large amounts of latent heating (Hirata et al., 2019), with the latent heating and availability of moisture being a strong controlling factor on the rate of intensification as a cyclone develops (Reed et al., 1988; Ahmadi-Givi et al., 2004). As a result of the rapid intensification, these cyclones often achieve a high peak intensity and can be associated with both strong winds and extreme precipitation (Browning, 2004).

In the Northern Hemisphere, bomb cyclones primarily form over the warm western margins of the Atlantic and Pacific during DJF (Fig. 8a), but there are also clear formation areas to the east of high topography over North America and East Asia, as was the case for all cyclones (Fig. 6a). The frequency of bomb cyclogenesis reduces in the Northern Hemisphere during spring (Fig. 8b) with formation restricted to the western boundaries of the ocean basins. Very few bomb cyclones occur in the summer (Fig. 8c), but activity increases in the Northern Hemisphere during the autumn (Fig. 8d) primarily in the western margins of the Atlantic and Pacific Oceans.

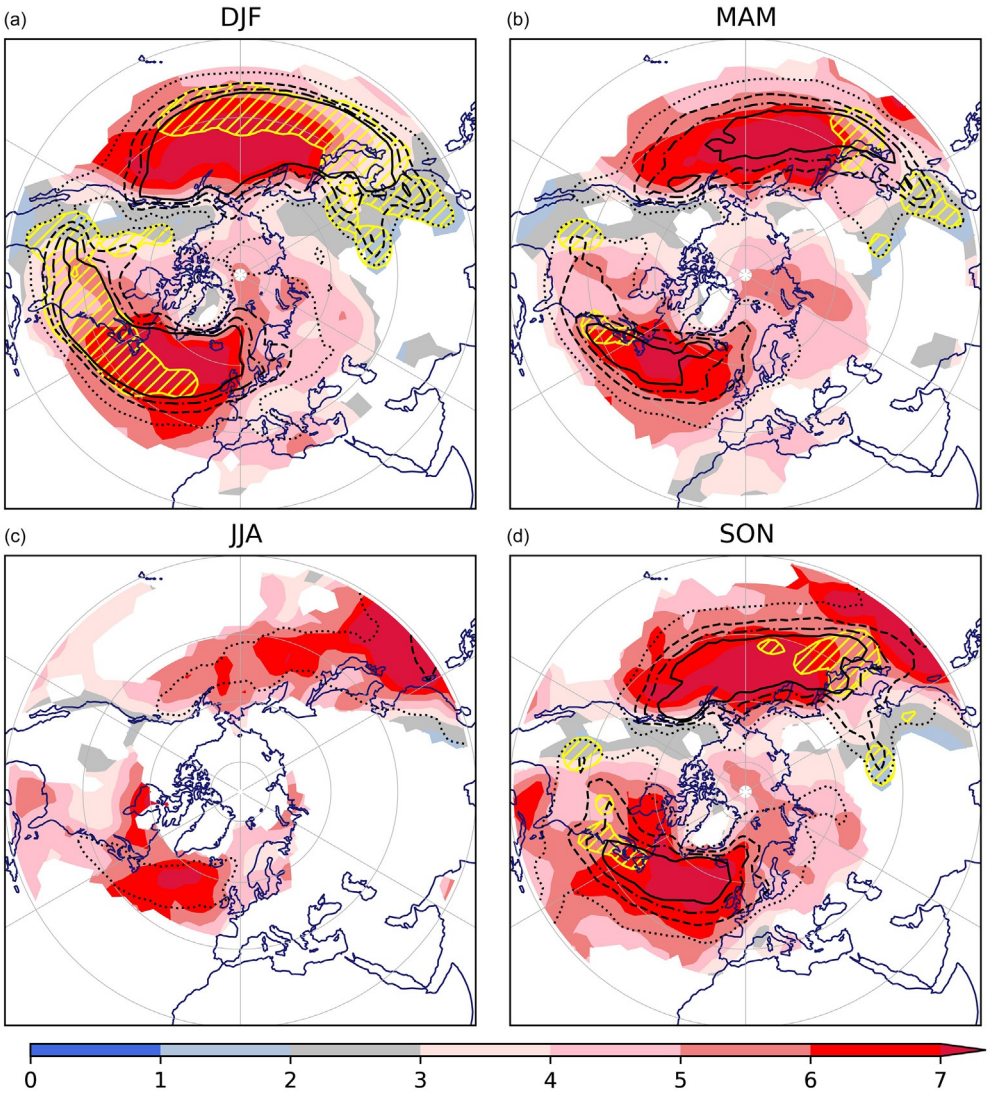

Fig. 8 Mean bomb cyclone track density (contours, dotted at 0.5, dashed at 1.5, dot-dashed at 2.5 and solid at 3.5), genesis density (yellow hatching for greater than 0.3) and mean intensity (shading, s^{-1}) from ERA5 1980–2022 in the Northern Hemisphere for positive vorticity features identified in the 850 hPa wind and mean sea level pressure fields using TRACK (see Priestley et al., 2020, and references therein). (a) December-January-February (DJF), (b) March-April-May (MAM), (c) June-July-August (JJA) and (d) September-October-November (SON). For track and genesis density, the units are number per month per 5° spherical cap. Mean intensity shading has been masked out where track densities are less than 0.1 (akin to Figs. 6 and 7). Map lines delineate study areas and do not necessarily depict accepted national boundaries.

Southern Hemisphere bombs are ubiquitous features with high track densities throughout the year (Fig. 9a–d). The highest bomb cyclogenesis rates occur in a band from the lee of the Andes to the south of Australia in JJA (Fig. 9c), which coincides with strong sea surface temperature gradients (Lim and Simmonds, 2002). The band becomes more fragmented in the other seasons, with the lowest genesis rates in DJF (Fig. 9a); however, the region to the lee of the Andes appears to be favorable for formation throughout the year.

Due to their high intensities, the impacts from bomb cyclones can be significant, with notable historic storms being those that have explosively deepened. The Great Storm of 1987 was a notable bomb cyclone (Burt and Mansfield, 1988), in which 22 people lost their lives, an estimated 15 million trees were uprooted, and resulted in an estimated €9 billion in insured damages in the UK (2022 equivalent; Cusack, 2023). A more recent occurrence was Storm Cíaran in November 2023, which caused 21 fatalities and approximately €2 billion in insured losses over areas of northwestern Europe (PERILS, 2024). The high peak intensity of these storms means that they pose a significant risk if they impact land, and especially in densely populated areas such as western Europe, or the west coast of North America.

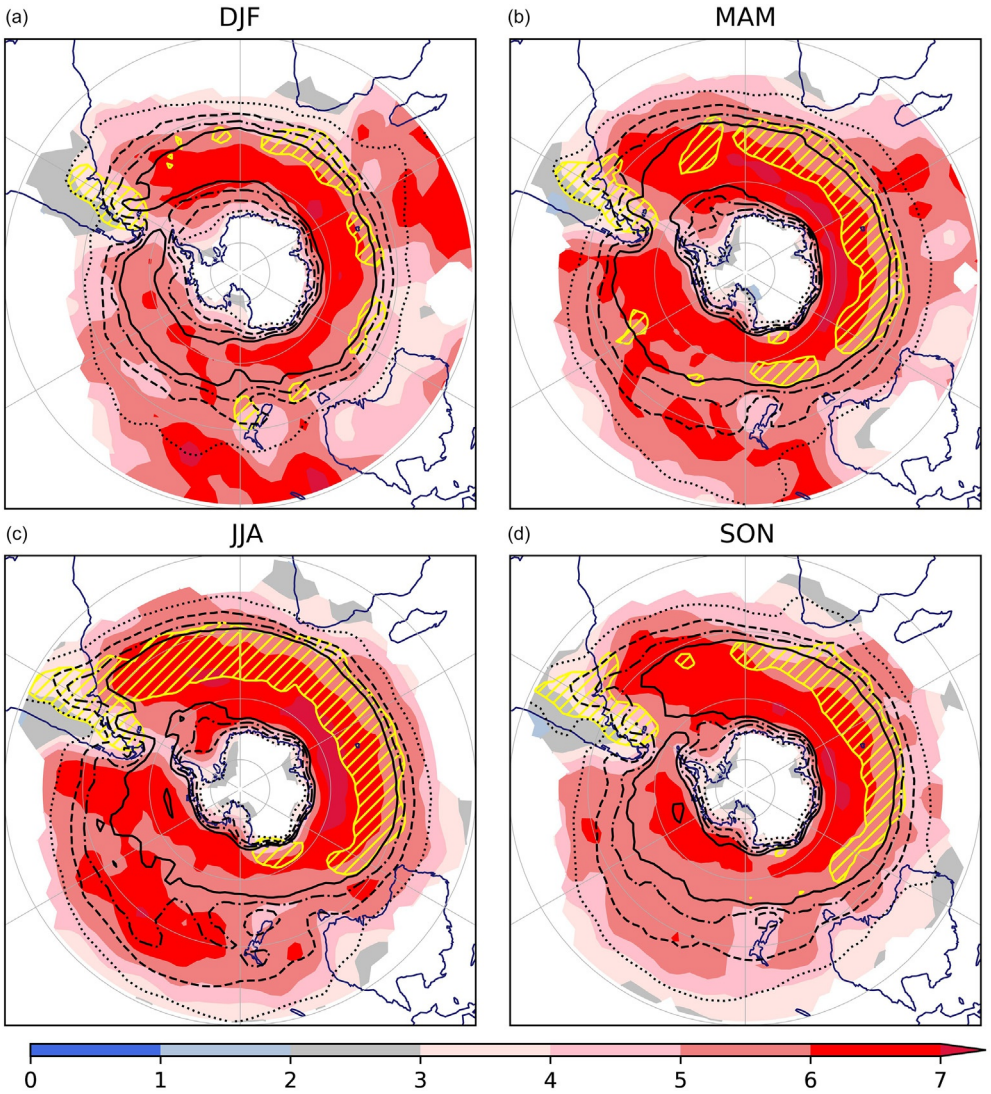

Fig. 9 The same as Fig. 8 except for the SH. Map lines delineate study areas and do not necessarily depict accepted national boundaries.

Lee cyclones

Given the prevalence of cyclogenesis in the lee of high topography in Figs. 6–9, it is important to discuss lee cyclone structure and associated weather. Lee cyclones may develop in both terrestrial (e.g., in the lee of the Rocky Mountains over North America) or marine (e.g., in the lee of the Alps near the Mediterranean Sea) environments, and examples of both are described here.

The development of deep extratropical cyclones in the lee of the Alps generally begins with the approach of an existing cyclone to the north over Europe (see Schär, 2003 for a comprehensive review). Typically, the cold front from the extratropical cyclone impinges on the northern Alpine slopes with warm, moist south-westerly flow from the Mediterranean Sea along the southern slopes. The combination of the south-westerly flow being forced to ascend over the Alps and the progression of the cold front from the north being blocked by the Alps, results in a shallow mesoscale low developing on the southern side of the mountains. For the cyclone to intensify, the presence of an approaching upper-level trough is vital to deepen the low-level mesoscale circulation throughout the troposphere. The deep lee cyclone may then propagate away from the mountain range with the upper-level trough and take on the characteristics of a typical frontal extratropical cyclone (Norwegian or Shapiro-Keyser).

Lee genesis along the eastern edge of the North American Rocky Mountains differs to the Alps for two reasons. First, the Rocky Mountains are orientated perpendicular to the prevailing westerly flow (the Alps are more parallel). Second, genesis occurs over land, which includes the presence of strong moisture (i.e., a moisture discontinuity known as a "dry line") and thermal gradients, which results in a different structure to both the Norwegian and Shapiro-Keyser models (see Fig. 10), as detailed in Hobbs et al. (1996). As with Alpine lee cyclogenesis, an approaching mid-to-upper level (250–500 hPa) trough on the western slopes of the Rocky Mountains supports the development of a pressure trough on the eastern side. The trough draws warm, moist air poleward from the Gulf of Mexico, which converges with the dry downslope flow from the Rocky Mountains. The dry air that descended from

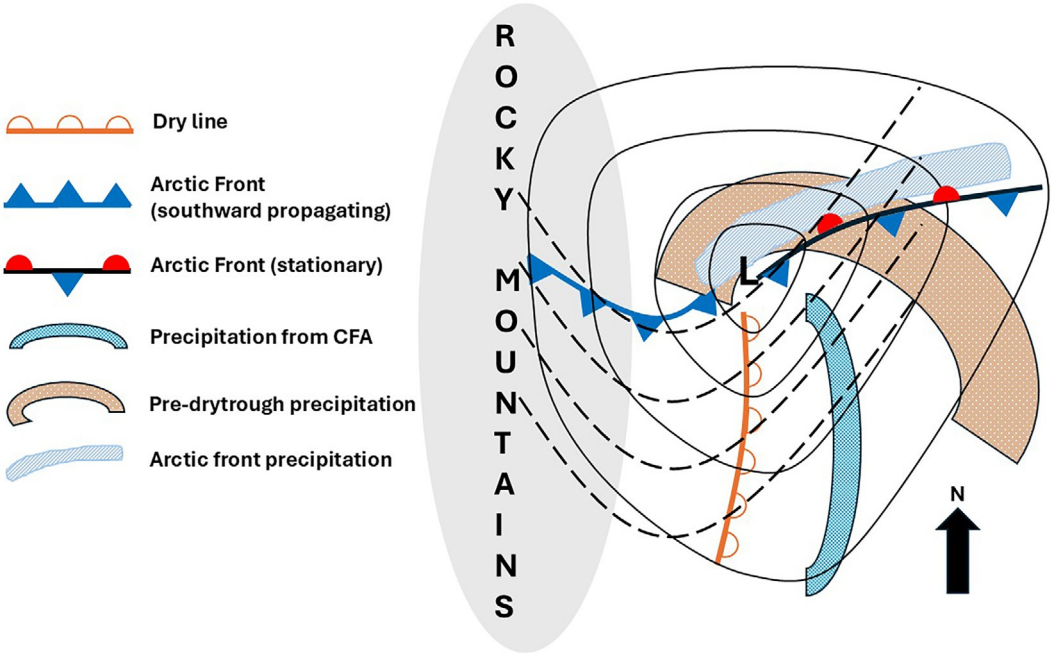

Fig. 10 Structure of a mature cyclone in the lee of the Rocky Mountains (gray shading), north indicated by the black arrow on the bottom right). The legend describes the components of the surface cyclone with the upper-level geopotential height trough indicated by the dashed lines (heights decrease from south to north). The "L" refers to the surface pressure minimum of the cyclone with the solid lines representative of surface isobars decreasing towards the L. Adapted from Hobbs PV, Locatelli JD, and Martin JE (1996) A new conceptual model for cyclones generated in the Lee of the Rocky Mountains. *Bulletin of the American Meteorological Society* 77: 1169–78. https://doi.org/10.1175/1520-0477(1996)077<1169:ANCMFC>2.0.CO;2.

the Rocky Mountains then ascends over the moister air leading to potential instability. This instability can be released far away from the surface moisture boundary and form a "pre-dry trough precipitation band" as depicted in Fig. 10. Furthermore, as the upper-level trough crosses the mountain range and induces ascent ahead of it, another band of convective rain may form known as the "Cold Front Aloft" (see the Cold Fronts section) or CFA rain band. At lower levels on the northern flanks of the extratropical cyclone, a band of stratiform precipitation may develop as warm, moist air to the south is advected poleward and ascends over the cold Arctic air. As the precipitation falls into cold, Arctic air, hazards associated with snow and freezing rain frequently occur. Furthermore, the pre-dry trough precipitation band may overlie the Arctic front precipitation and increase the snow and freezing rain hazards. As for the southward propagating portion of the Arctic front on the western flank of the cyclone, there is generally little precipitation associated with this as relatively dry air behind the dry line is lifted. As can be seen from this description, cyclones developing in the lee of the Rocky Mountains (and conceivably in the lee of the Andes too) may have a very different structure to those developing over the ocean (as with both the Norwegian and Shapiro-Keyser models).

Cyclone relative air flows

From the descriptions above, extratropical cyclones develop in a non-stationary background flow and propagate through it. This complex, non-stationary synoptic-scale flow combines with the cyclonic motion of air around the cyclone center and the vertical motion within it. The use of a Lagrangian (i.e., following the flow) point of view, therefore, provides invaluable insight on the structure of cyclones, air mass boundaries and frontal structures and their lifecycle. With this perspective, air masses can be tracked in 4-dimensions (space and time) through evolving extratropical cyclones and used to identify recurring airstreams (Wernli, 1997). Based on several illustrative cyclone case studies, a conceptual model of three coherent airstreams emerged (Carlson, 1980): the warm and cold conveyor belts and the dry stream (later referred to as the dry intrusion). With the availability of 4-dimensional global circulation and thermodynamic datasets, studies over the last four decades have employed the Lagrangian view to compute full airmass trajectories of the airstreams associated with extratropical cyclones. A conceptual model of the three main airstreams, together with the sting jet, can be seen in Fig. 11 with each discussed in more detail below.

Warm conveyor belt (WCB)

The warm conveyor belt (WCB) is depicted in Fig. 11 by the red arrows. The WCB is a warm and moist ascending airstream that transports heat and moisture polewards from the boundary layer at low latitudes to the upper atmosphere. The lower tropospheric portion of the WCB corresponds to high wind speeds along the cold front known as the "warm jet" (indicated by the red oval in Fig. 11) and occurs during the initial stages of cyclone development (Hewson and Neu, 2015). As the WCB air from the warm sector

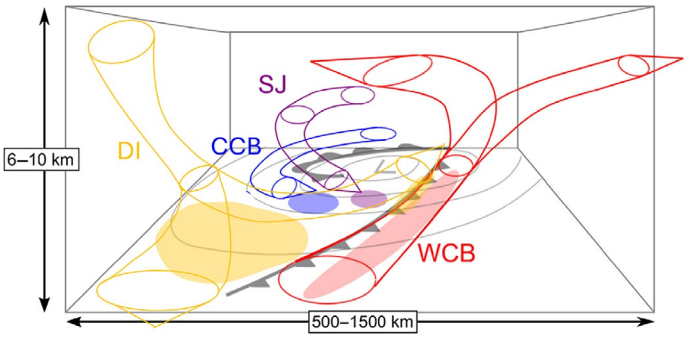

Fig. 11 Conceptual model of the 3D structure of a Shapiro-Keyser cyclone showing the warm conveyor belt (WCB, red), cold conveyor belt (CCB, blue), dry intrusion (DI, yellow) and sting jet (SJ, magenta). In each case the region of strong surface winds is indicated by the shading. Adapted from Clark PA, Gray, S.L., 2018. Sting jets in extratropical cyclones: A review. Quarterly Journal of the Royal Meteorological Society, 144(713), 943–969.

moves poleward and ascends, saturation and condensation of water vapor occurs releasing large quantities of latent heat. The latent heating may add ~20 K to the potential temperature of the air, thereby significantly boosting ascent (Wernli, 1997; Joos and Wernli, 2012). From this, the accepted Lagrangian definition for WCB flow is for air parcels to ascend at least 600 hPa in a 48-h time window in the vicinity of a cyclone (Madonna et al., 2014). Towards the end of the ascending branch of the WCB, the condensation of water vapor and further freezing of water results in a typical hook-shaped cloud pattern, as the WCB flow spreads and curves cyclonically and/or anticyclonically around the cyclone center (red arrow heads in Fig. 11).

Atmospheric river (AR)

At the base of the WCB airstream there are often filaments of enhanced water vapor transport, seen in satellite images as elongated cloud features that often extend from the subtropics to the extratropics. Referred to as "atmospheric rivers" (ARs), they are directly related to water supply and flooding potential once the moist air ascends in the WCB and/or upon hitting high orography (Gimeno et al., 2014). However, differently from what their name suggests, ARs are not a Lagrangian flow feature. As such, their moisture source is not necessarily the distant tropics or subtropics, but rather moisture that evaporated locally and the AR flow picks up (Dacre et al., 2015).

Cold conveyor belt (CCB)

The cold conveyor belt (CCB) marks the cyclonic flow on the cold (poleward) side of the warm front (the blue arrow in Fig. 11). This lower-tropospheric airstream flows rearward relative to the motion of the cyclone with only weak (or no) ascent. In late stages of cyclone development, CCB trajectories wrap cyclonically around the cyclone center, align with the cyclone's motion and descend, thereby inducing strong surface winds behind the cold front (Schultz, 2001; Martínez-Alvarado et al., 2014; Hewson and Neu, 2015; Raveh-Rubin and Wernli, 2016). The near-surface wind signature from the CCB can be distinct or overlap with that of the sting jet (see the Sting Jet section).

Dry intrusion (DI)

The dry intrusion (DI) airstream is marked by the slantwise descent of dry air on the rearward side of the cyclone (Wernli, 1997; Browning, 1997). In DIs, air originates from the upper troposphere (or occasionally from the lower stratosphere), descends coherently into the cyclone cold sector, and fans out behind the cyclone's trailing cold front (yellow arrows and shading in Fig. 11). The DI descent is less pronounced than the counterpart ascent within the WCB, resulting in a descent threshold of at least 400-hPa descent within 48 h and serves as a Lagrangian identification criterion for DIs (Raveh-Rubin, 2017).

Near the cyclone center, the dry and cold air overruns the warm and moist air ahead (yellow arrow overrunning the cold front in Fig. 11) in the so-called "dry slot," inducing potential instability that can lead to deep convection and cyclone deepening (Browning, 1997; Young et al., 1987). Furthermore, away from the cyclone center, DIs are associated with strong trailing cold fronts and deepened boundary layers (Catto and Raveh-Rubin, 2019; Ilotoviz et al., 2021). The high-momentum upper-tropospheric air is transferred into the cold sector at low levels, resulting in overall enhanced cold and dry wind anomalies there (yellow shading in Fig. 11).

The surface anomalies induced by the DI are important components for the association of the cyclone and frontal passage with severe surface weather. Namely, DIs are directly related to surface cold extremes (Klaider and Raveh-Rubin, 2023), strong winds (Browning and Golding, 1995; Givon et al., 2024), fire weather (Magaritz-Ronen and Raveh-Rubin, 2023) or Saharan dust emissions (Fluck and Raveh-Rubin, 2023).

Sting jet

Browning (2004) coined the term "sting jet" (SJ) for the transient mesoscale airflow causing the most damaging winds in extratropical cyclones. In their review of observational and modelling studies of SJs since then, Clark and Gray (2018) define the SJ as "a coherent air flow that descends from mid-levels inside the cloud head into the frontal-fracture region of a Shapiro-Keyser cyclone over a period of a few hours leading to a distinct region of near-surface stronger winds." Thus, for SJs to develop, a frontal fracture is required (as seen Shapiro-Keyser cyclones), where air rapidly descends from the cloud head into the dry slot at the mesoscale (indicated by the magenta arrow in Fig. 11). The high-momentum SJ creates wind peaks in the lower troposphere that may penetrate the boundary layer top and reach the surface by convective circulations ahead of the CCB (Browning et al., 2015).

Fronts

The previous section described where the main flow features lie within an extratropical cyclone during its lifecycle; however, the boundaries between those flows (i.e., the fronts) have not been discussed in detail. Furthermore, given that the sections above also clearly show that fronts are an important feature of most extratropical cyclones (Schemm et al., 2018), a deeper description of them is required. Fronts are also integral to weather in the mid-latitudes where they typically occur on more than 20% of the days in a year (see Fig. 12 and Catto et al., 2012). As can be seen in Fig. 5, the typical fronts within a midlatitude cyclone are a warm front ahead of the cyclone center, and a cold front that either lies meridionally, or trailing zonally behind the cyclone. Sometimes, in the mature stage of a cyclone, an occluded front occurs. Therefore, a deeper dive into the structures of those weather fronts described above, along with other types of fronts (dry line, stationary, and Arctic fronts), are presented below.

The term "front" comes from the idea of two different air masses battling at some boundary, for example between a cold polar air mass and a warm tropical air mass (as in the polar front of the Norwegian model, see Fig. 5a). A front can therefore be thought of as a region of increased temperature or density (e.g., moisture) gradients. Fronts also exhibit changes in horizontal wind direction, changes in surface air pressure, cloud cover and precipitation. Moreover, they are associated with more than 50% of the precipitation in the mid-latitudes (Fig. 12 shading) and are therefore a key water resource for many communities there. The sections below describe several mechanisms of frontal development (frontogenesis) before discussing each type of front from a conceptual viewpoint.

Frontogenesis

The Norwegian model considers the polar front to be a pre-existing structure on which cyclones can grow (Fig. 5(a)I); however, such a situation is not necessary as the atmospheric circulation can act to increase temperature gradients locally through a process called frontogenesis. Kinematically, the atmospheric flow alone can act to increase temperature gradients and thereby induce frontogenesis, by:

1. Stretching (Fig. 13a): confluent flow (i.e., where streamlines come together) acts to direct cold air on the cold side of the front and warm air on the warm side of the front closer together, thereby squeezing the isotherms together.

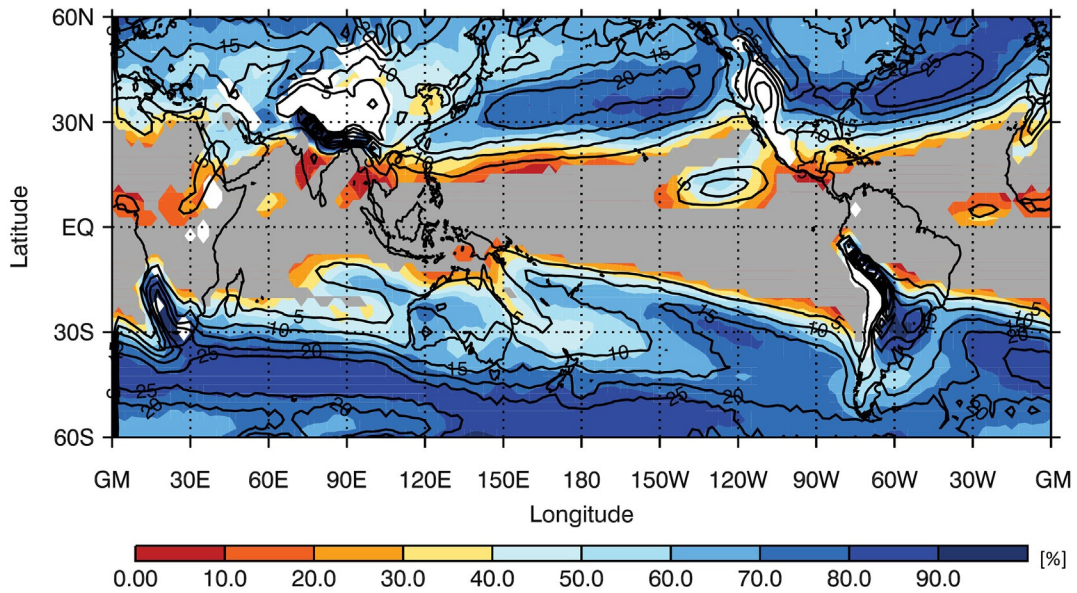

Fig. 12 The annual mean frequency of fronts identified in a reanalysis dataset (ERA-Interim) shown by the black contours, and the proportion of total 24-h precipitation associated with fronts shown by the colors. Map lines delineate study areas and do not necessarily depict accepted national boundaries. Figure adapted from Catto JL, Jakob C, Berry G, and Nicholls N (2012) Relating global precipitation to atmospheric fronts. *Geophysical Research Letters* 39: L10805. https://doi.org/10.1029/2012GL051736. Copyright 2012 by the American Geophysical Union.

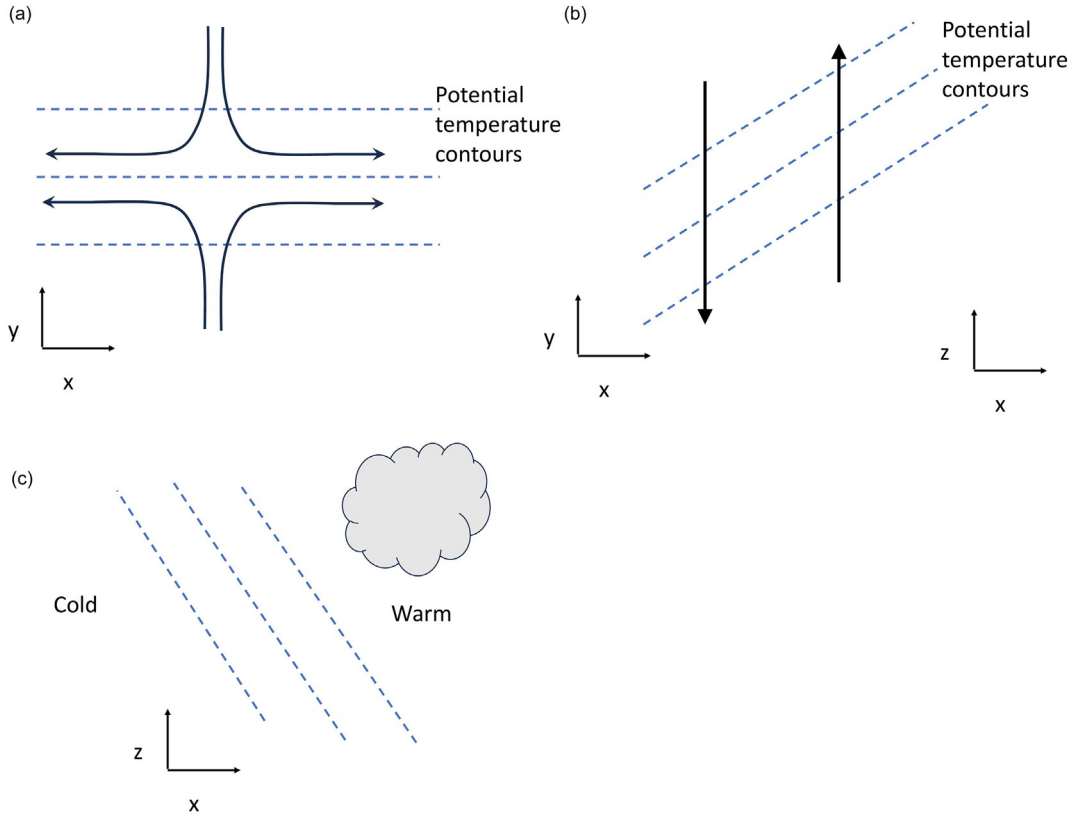

Fig. 13 Mechanisms of frontogenesis. (a) Stretching, (b) shearing, (c) diabatic frontogenesis. Isotherms (potential temperature) are indicated by the dashed lines with the flow indicated by the black arrows. The cloud in (c) is described in an example in the text and is indicative of diabatic processes.

2. Shearing or tilting (see Fig. 13b): in the horizontal plane, flow in opposite directions at some angle to the isotherms induce shearing frontogenesis, with a similar process occurring in the vertical (called tilting).

Differential heating (diabatic processes) on opposing sides of a front can also cause the temperature gradient to increase (or decrease). For example, night-time cooling in clear air on the cold side of a front, and reduced cooling due to the presence of cloud on the warm side may cause the temperature gradient to increase across the frontal boundary, initiating frontogenesis (Fig. 13c).

As frontogenesis occurs, a secondary circulation is induced in the vertical, with ascent in the warm air and descent in the colder air (i.e., a thermally direct circulation). This thermally direct cross-front circulation acts to increase the temperature gradients further. When geostrophic theory is applied to frontogenesis (Fig. 14a—top row), only the geostrophic flow (purple arrows, Fig. 14a) can act to strengthen the temperature gradient with time whereas the ageostrophic component has no impact on the thermal gradient (red arrows, Fig. 14a). Geostrophic frontogenesis therefore results in only low-level strengthening of the temperature gradients. An alternative, known as semi-geostrophic theory[2] (Hoskins, 1975), which accounts for the long and narrow nature of frontal systems, is necessary to explain observed frontogenesis (Fig. 14b—bottom row). In semi-geostrophic theory the along front wind is assumed to be in geostrophic balance, but the across front circulation has a significant ageostrophic component, which results in a stronger and deeper frontal boundary (compare Fig. 14b with Fig. 14a). As with extratropical cyclones, it is this important ageostrophic component of the wind that is key for frontal development.

All these different mechanisms described above may occur separately or concurrently during frontogenesis; however, further consideration of the direction of frontal propagation and vertical structure is needed to identify the type of front that is developing. The characteristics of the three most prevalent frontal types are now considered along with three other less common (but highly relevant) fronts.

Cold fronts

At a cold front, cold air advances towards relatively warm and moist air, forcing the ascent of the air ahead. This ascent can be quite rapid, so that cold fronts can often be associated with deep clouds and heavy precipitation. The ascending air typically follows two different paths: in "anafronts," there is rearward sloping ascent at the cold front (see Fig. 15a); in "katafronts," there is forward

[2]https://glossary.ametsoc.org/wiki/Semigeostrophic_theory.

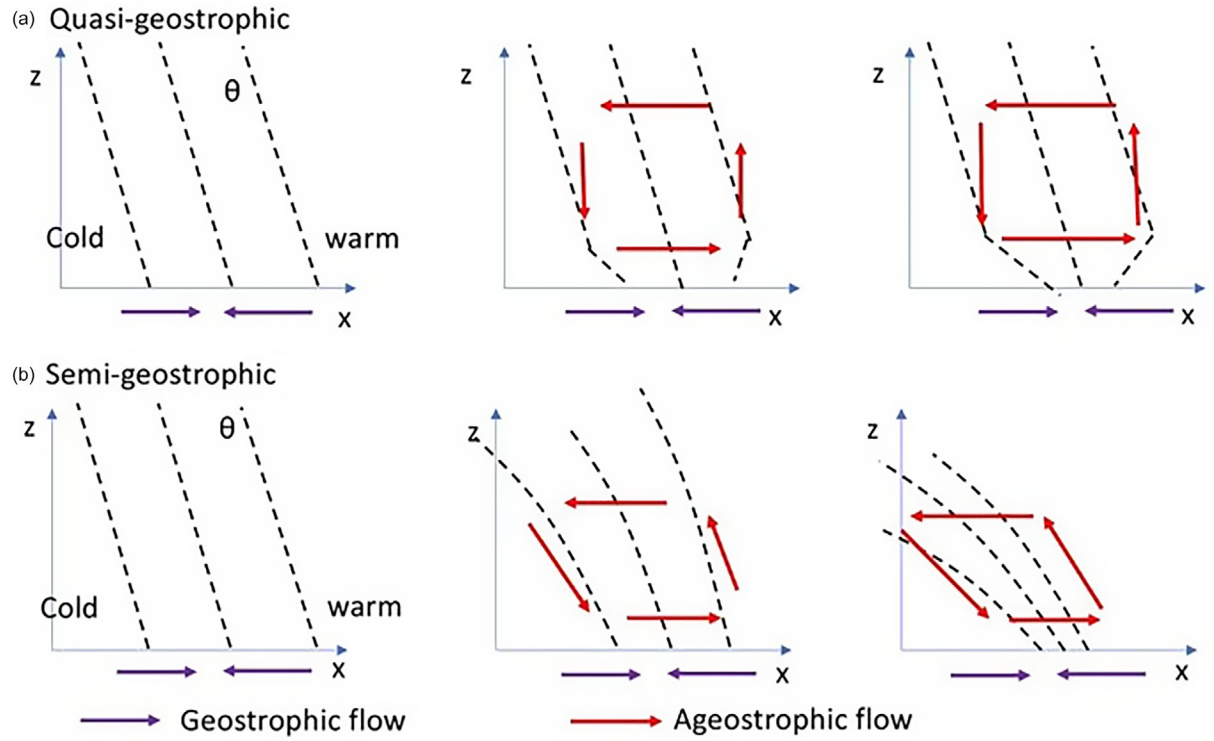

Fig. 14 Quasi-geostrophic (a) versus semi-geostrophic (b) frontogenesis through time (left to right). In Quasi-geostrophic theory, only the geostrophic flow enhances the temperature gradients at the surface. In semi-geostrophic theory, the ageostrophic flow can also contribute to the frontogenesis. Dashed lines indicate isotherms (potential temperature), geostrophic (purple) and ageostrophic (red) flows are indicated by the arrows.

sloping ascent (see Fig. 15b). These flows are associated with different surface weather; anafronts have very heavy precipitation, whereas katafronts have weaker precipitation at the surface due to the overrunning, descending drier air. Strong winds are also frequently found on the warm side of both ana and kata cold fronts, where the pressure gradients are strong. These regions contain low-level jet streams, which are associated with the inflow of the warm conveyor belts (see the Cyclone relative air flows section).

Upper-level cold fronts (or CFAs, as described in the Lee Cyclones section) are also a feature of mid-latitude weather (Fig. 10) and are regions of strong temperature gradients away from the surface. Such upper-level cold fronts are typically associated with tropopause folds (significant incursion of air from the stratosphere to lower levels) and an example is shown schematically in Fig. 16a. These tropopause folds are associated with the core of the upper-level jet where both horizontal and vertical process lead to strong descending motion. Surface fronts can be impacted by upper-level fronts by either coupling with the low-level circulation, which contributes to the release of convective instability (Fig. 16b), or by being uncoupled (Fig. 16c) (also see Keyser, 1999).

As can be seen from Figs. 15 and 16, cold fronts can have complex and varied structures. Such structural variations can lead to many types of hazardous weather. For example, regions of enhanced cloudiness and precipitation known as "mesoscale rainbands" may form in areas of conditional symmetric instability. Other mesoscale features within cold fronts include:

- Cloud striations: convective features that sit above the main cloud band (Browning and Wang, 2002).
- Line convection: A narrow band of strong vertical ascent associated with anafronts that may extend for hundreds of kilometres along the front (Browning, 1990, and references therein)

These can be associated with high impact surface weather such as heavy precipitation or wind gusts. Depending on the region of the world, cold fronts can also be associated with intense thunderstorms, or even tornadoes.

Warm fronts

Warm fronts exist where warm, moist air moves towards relatively colder air (see Fig. 17). The warm (less dense) moist air ascends in a slantwise fashion (depicted by the red arrows in Fig. 17) over the colder (denser) air. A much broader region of stratiform cloud (gray shading, Fig. 16) is created with cirrus at the leading edge and precipitation (vertical lines, Fig. 17) from nimbostratus near the surface front. As the air rises over the warm front it may turn cyclonically (middle two arrows Fig. 17) around the cyclone center, or anticyclonically when it gets entrained in the upper-level jet (top arrow in Fig. 17), as part of the larger-scale warm conveyor belt. Warm fronts in Shapiro-Keyser cyclones tend to have a stronger thermal gradient and precipitation than Norwegian Model cyclones.

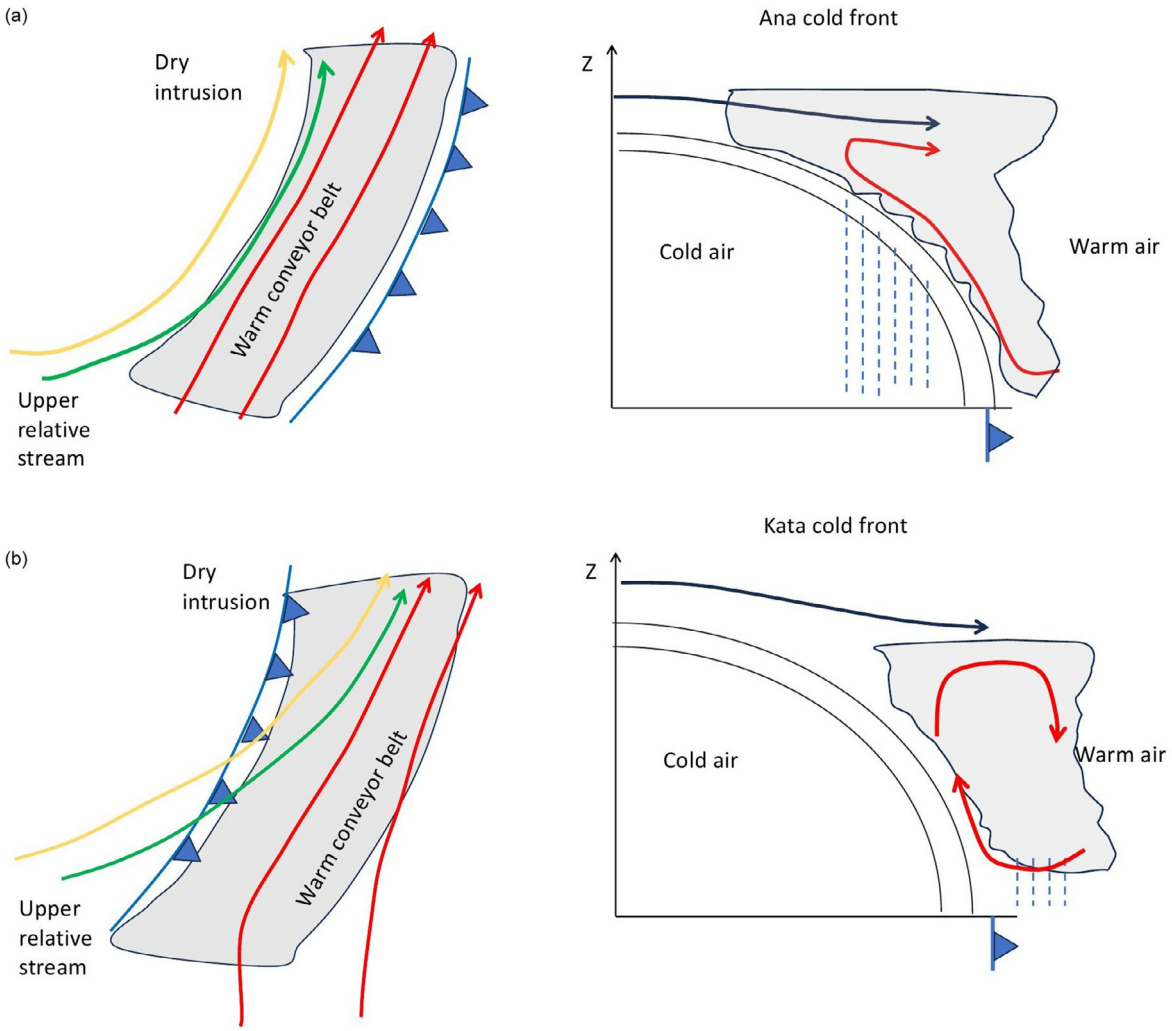

Fig. 15 Ana (a) and kata (b) fronts in plan view (left) and in vertical cross-section (right). For the plan views (left), the arrows are indicative of the dry intrusion (yellow), upper air (green) and warm conveyor belt (red) flows. For the vertical cross sections (right) the arrows indicate the upper level (blue) and transverse warm conveyor belt (red) flows. Precipitation is indicated by the blue dashes, cloud is shaded gray, and the surface front is denoted by a blue line with triangles.

Occluded fronts

Occluded fronts were originally included in the Norwegian model of cyclone lifecycles (see Fig. 5a). The main feature of an occluded front is the warm sector air being lifted away from the surface, resulting in a weaker surface temperature gradient (Fig. 18). This was initially described as the "catching up" of the cold front with the warm front and would give two types of occlusions; a cold-type occlusion where the air behind the cold front is colder than the air ahead of the warm front (Fig. 18a); and a warm-type occlusion where the air behind the cold front is warmer than the air ahead of the warm front (Fig. 18b). However, the idea of the cold front catching up with the warm front fails to explain several features of occluded fronts, such as the possibility of observing an occlusion in Shapiro-Keyser-type cyclones, and the presence of long fronts isolated from a parent cyclone. The concept of the fronts wrapping up in the cyclonic circulation provides a more generalized understanding of the occlusion process (Schultz and Vaughan, 2011). Significant cloud and precipitation can be associated with an occlusion, which often line up closely with the trough of warm air aloft known as a trowel (see Fig. 18b and Martin, 1999).

Other mid-latitude fronts

While cold, warm and occluded are the most prevalent types of fronts, there are other frontal structures that are important for mid-latitude weather that have been described briefly in the Lee Cyclones section. These other types of fronts, presented in Fig. 10, are known as a dry line, a stationary front and an Arctic front. The main characteristics of each of these fronts are:

- Dry lines: Where there is a significant change in the moisture properties of the atmosphere. As the front passes there may only be a small increase in the air temperature; however, there is a marked reduction in humidity and perhaps a change in wind

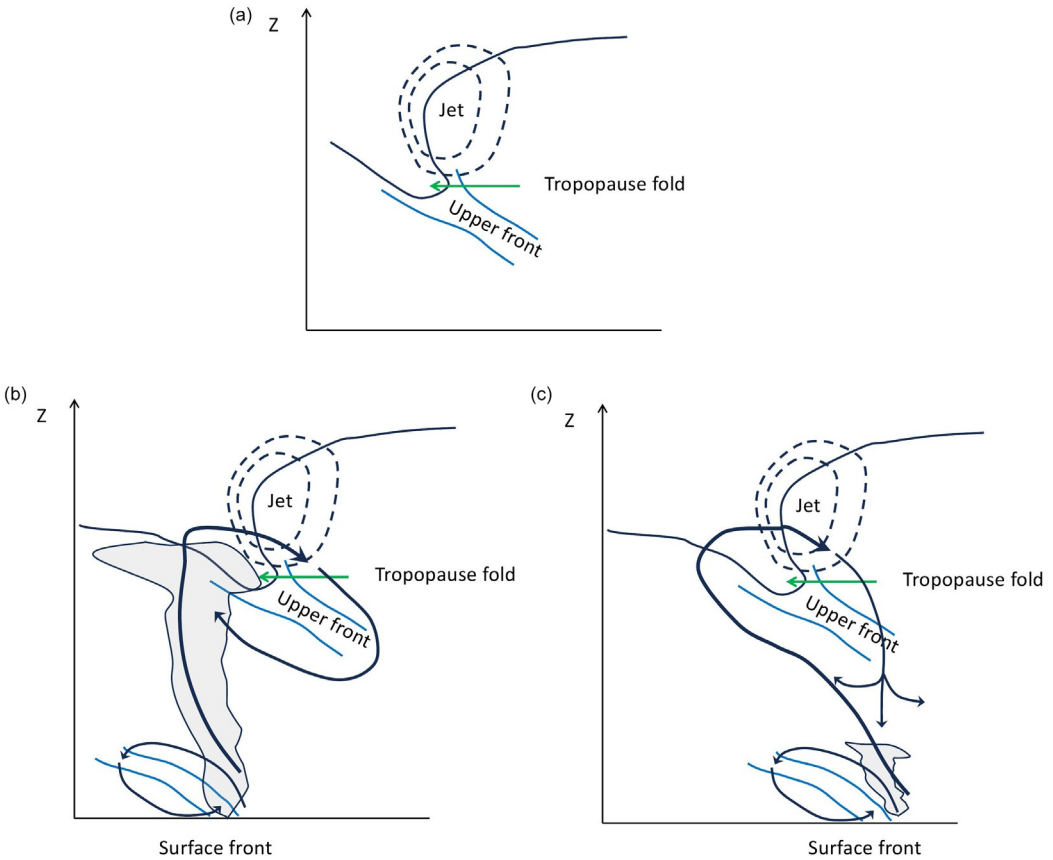

Fig. 16 Upper-level fronts following the work by Keyser (1999). (a) the general picture of an upper-level front, (b) where there is significant release of convective instability, (c) where the upper-level front results in suppression of convection. The tropopause is indicated by the solid, black line; the upper-level jet is indicated by the black, dashed lines, frontal surfaces are denoted by the solid blue lines; shading is indicative of cloud; the arrows indicate the main circulations.

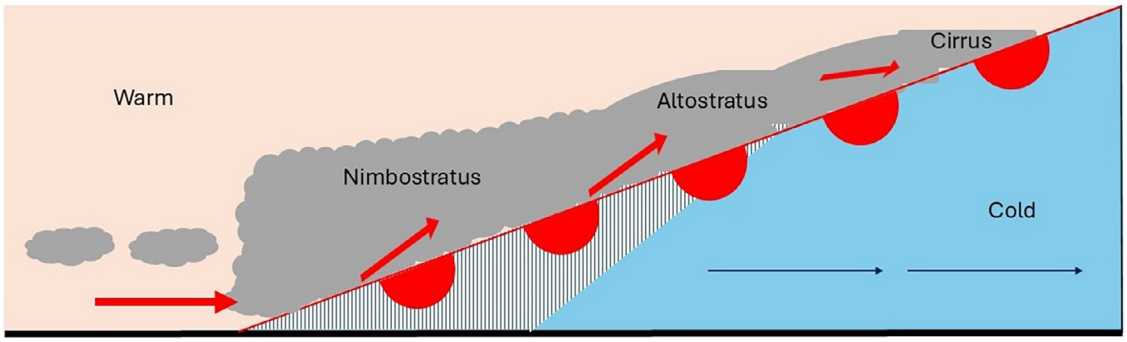

Fig. 17 Vertical cross section of a warm front (red line and scallops) moving from left to right. The arrows are indicative of cold (blue) and warm (red) air flow. The middle two red arrows are turned to indicate a cyclonic turning of the wind up to mid-levels, with the top arrow indicative of anticyclonic turning of the wind at upper levels (corresponding to the flow of the WCB). Cloud is shaded gray with precipitation denoted by vertical lines.

direction. The drier air is lofted over the moister air leading to potential instability, which is conducive to severe thunderstorm development.

- Stationary fronts: A stationary front occurs where two air masses converge on each other from opposing directions. The resulting air flow tends to be parallel to the frontal surface but in opposing directions. There is little propagation perpendicular to the frontal boundary. A stationary front may remain over a given area for several days.
- Arctic fronts: A very shallow feature akin to a density current with a rapid drop in air temperature, but little precipitation associated with it. A common feature in North American extratropical cyclones where very cold Arctic air is drawn south along the eastern slopes of the Rocky Mountains and displaces cool, dry air ahead of it.

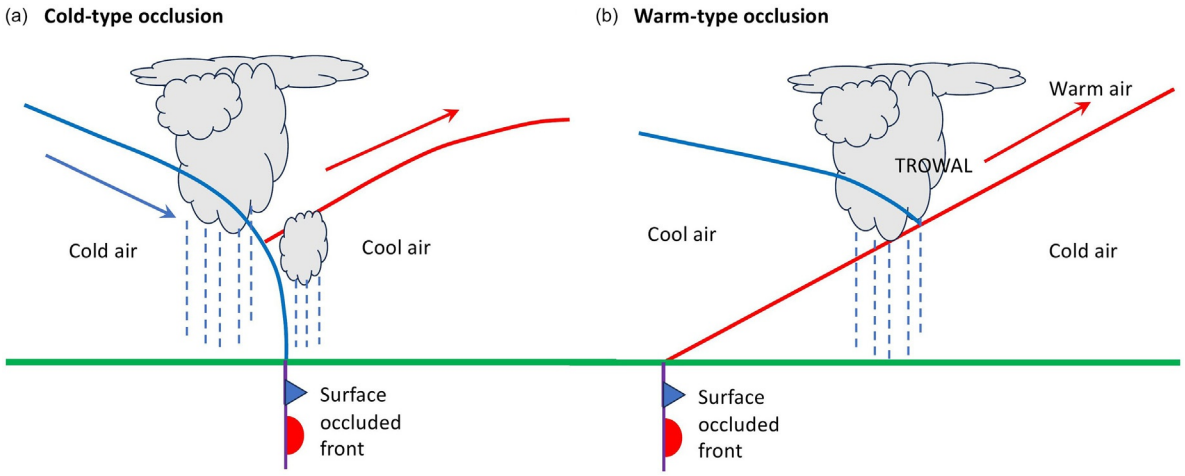

Fig. 18 Cold-type (a) and warm-type (b) occluded fronts. In (b) the trough of warm air aloft can be seen as the location of significant precipitation.

There are also other local circulation features that can be considered as fronts (e.g., a sea breeze front); however, their description is beyond the scope of this article.

Cut-off lows

The previous sections have described the main development mechanisms, location and sub-synoptic features of extratropical cyclones; however, there has been no discussion of what happens as the cyclone decays and the initial thermal gradient has diminished. Once the cyclone has become cut off from the influence of the surface thermal gradient and upper-level jet, a cut off low may form. A schematic for highlighting the main concepts and processes involved in the development of a cut-off low is shown in Fig. 19 and further discussion of such lows can be found in Muñoz et al. (2020, and references therein). An upper-level trough may amplify over time (Fig. 19a and b), for example if it becomes phase-locked with a developing surface low pressure system. Further amplification of the upper-level trough may eventually lead to the formation of a circular geopotential height minimum (denoted "L" in Fig. 19c), which then becomes cut-off from the main upper-level westerly flow (Fig. 19d), which is then defined as a cut-off low. While the salient features are shown in this highly idealized schematic, their horizontal scale can be affected by shear across the jet with those following LC1 paradigm smaller and more equatorward than those of LC2 (see Thorncroft et al., 1993). Furthermore, while cut off lows may be considered the end of the lifecycle of an upper level baroclinic wave, it does not mean they do not cause impactful weather. Intense cut off lows still retain significant structure, which often includes (see Fig. 10 in Pinheiro et al., 2021, and references therein):

- A cold anomaly and closed cyclonic circulation in the middle atmosphere.
- Low-level instability, especially if the low drifts equatorward over high land or ocean temperatures (convection), particularly during the warm season.
- Ascent and precipitation at the leading edge of the circulation due to both vorticity and warm air advection.

Furthermore, cut-off lows tend to have low propagation speeds and can therefore remain stationary over the same location and bring multiple days of heavy precipitation resulting in flooding. For example, the exceptionally heavy precipitation and flooding over Central Europe in July 2021 was associated with a cut-off low and caused more than 180 deaths and €46 billion in damage

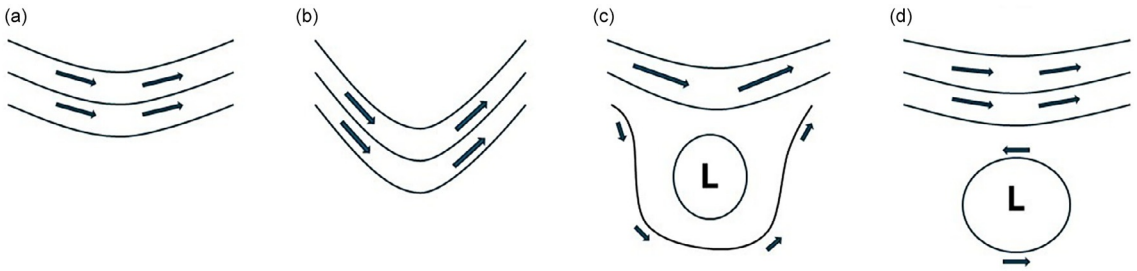

Fig. 19 Schematic of the development of a cut-off low. Solid lines indicate upper-level (ca. 300 hPa) geopotential height with arrows indicating the flow. The development of a small meander in the height field occurs (a), followed by amplification (b). A large meander in the flow develops with a closed geopotential height contour minimum indicated by the "L" (c) before the feature becomes cut-off from the prevailing westerly flow (d).

(Mohr et al., 2023). Cut-off lows are also prevalent in the Southern Hemisphere, such as the event that brought over 40 mm of rainfall and associated flooding to the hyperarid (i.e., <1 mm rainfall per year) Atacama Desert (Bozkurt et al., 2016).

Having described the development of an amplifying trough into a cut off low and its associated weather, troughs do not often appear in isolation. Large-scale ridges may form up and/or downstream of such amplifying troughs and go through their own amplification cycle. The development of such large-scale amplifying ridges may result in a phenomenon known as a "blocking anticyclone" (or a "block"), which is also a key feature of the mid-latitude weather (and the focus of the next section). One of the reasons therefore why cutoff lows may be so impactful, is that they form during a blocking regime and become stationary and thereby impact the same region for many days.

Blocking anticyclones

What is an anticyclone?

The other common weather feature in mid-latitudes, and the "opposite" to extratropical cyclones, is the anticyclone. At the surface, anticyclones are characterized by high atmospheric pressure and sinking air and generally calm winds. These winds spiral outwards from the center of the high in a clockwise direction in the Northern Hemisphere (see Fig. 1), and anticlockwise in the Southern Hemisphere. Unlike extratropical cyclones, anticyclones primarily consist of only one distinct air mass, with a more uniform distribution of temperature and humidity throughout the system than an extratropical cyclone. The large-scale descent within an anticyclone generally suppresses the development of deep, precipitation-bearing clouds, and as such anticyclones are normally associated with dry weather.

In mid-latitudes, anticyclones can be classified into two distinct groups: (1) transient anticyclonic "ridges" that travel along the jet stream with their cyclonic (extratropical cyclones) counterparts, and (2) quasi-stationary anticyclones, known as "blocks," that are not advected downstream by the large-scale circulation. Such anticyclones are known as blocks as they cause the mid-latitude circulation to become "blocked," which is then forced around the blocking anticyclone. When the jet stream is interrupted in such a way, extratropical cyclones are unable to progress eastwards as normal and instead stall as they reach the outer edge of a block. This is like traffic becoming stuck behind a blockage on a road—until the blockage is removed, traffic (or cyclones) cannot progress further down the road (or jet).

In the atmosphere, these blockages can form many shapes which are all commonplace on synoptic charts of the mid-latitudes. The five typical blocking configurations (which are the focus for the rest of this chapter) are shown in Fig. 20, and are described below:

- Stationary ridge (Fig. 20a): a large-scale, stationary ridge in the planetary-scale flow.
- Omega block (Fig. 20b): so-called because of the pattern the geopotential height contours make around the blocking system, characterized by a large blocking anticyclone flanked on both sides by smaller, stationary cyclones.
- Wave breaking (Fig. 20c and d): when a ridge overturns and tilts around a cyclone in either an anticyclonic or cyclonic direction (more details are given in a later section).
- Rex or dipole block (Fig. 20e): often found at block maturity, where a blocking anticyclone is situated directly poleward of a stationary cyclone.

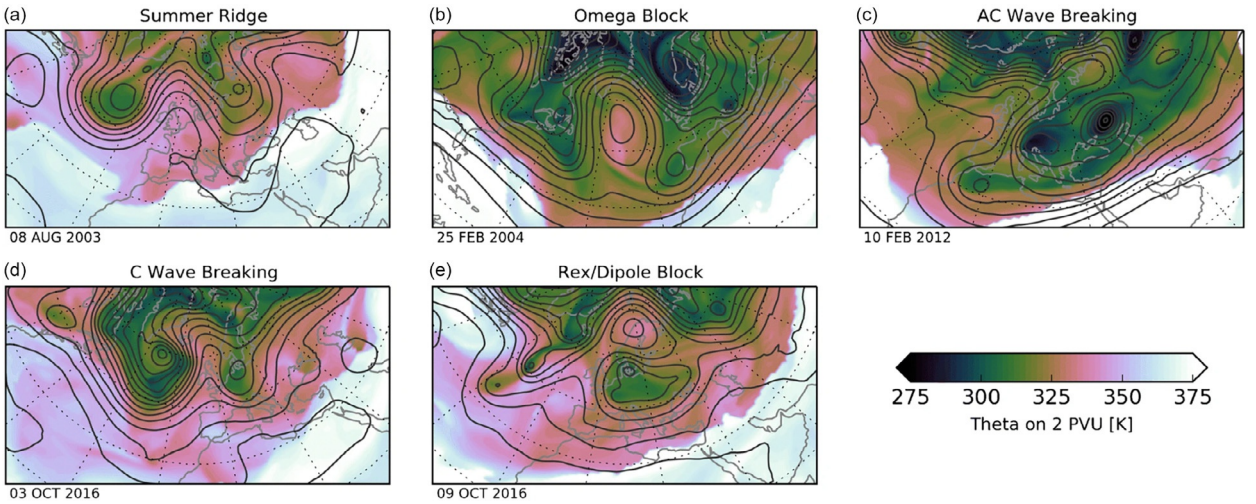

Fig. 20 Potential temperature on the 2 PVU surface (shading) and 500 hPa geopotential height (contours) for blocks of five different configurations. Map lines delineate study areas and do not necessarily depict accepted national boundaries. Figure from Woollings T, Barriopedro D, Methven J, Son S-W, Martius O, Harvey B, Sillmann J, Lupo AR, and Seneviratne S (2018) Blocking and its response to climate change. Curr Clim Change Rep, 4, 287–300.

Throughout its lifecycle, a block may take on the appearance of one or more of the above shapes. It should be noted that while not all individual blocks go through this lifecycle, a common morphology of blocking includes evolving from a ridge to an omega block, and then to a dipole block (Sousa et al., 2021).

What are blocking anticyclones?

Early idea development

Atmospheric blocking is a phenomenon that has piqued the interest of researchers for many decades, and one of the early studies into the subject was performed by Berggren et al. (1949). This study proposed an idealized pathway in which "unstable waves" develop into blocks, as shown in Fig. 21. Berggren et al. (1949) identified some notable characteristics of block development that are still shown to be important in modern-day studies, namely wave amplification (Fig. 21a–b), the cutting-off of a cold cyclone (Fig. 21c and d), retrogression (Fig. 21e), and a cold cyclonic intrusion from the northeast (Fig. 21f).

A year later, Rex (1950) identified that the main features that distinguish blocking anticyclones from transient ones are the following:

- *Persistence*. Blocks last longer than transient anticyclones, persisting for several days to several weeks.
- *Size*. Blocks are typically larger (width of several 1000 km) than transient anticyclones (around 1000 km).
- *Quasi-stationarity*. While transient anticyclones travel eastward as part of a ridge in a Rossby wave, blocking anticyclones are generally very slow moving or stationary, and can even sometimes retrogress and propagate westwards against the mean flow.
- *Vertical structure*. Blocks are approximately barotropic, i.e., the anticyclonic circulation is vertically stacked throughout the depth of the troposphere. On the other hand, transient anticyclones have a westward tilt with increasing height.
- *Effect on the jet stream*. Like a boulder in a river diverting the flow of water around it, blocks cause a disruption in the jet stream, causing it to split and divert to the north and south of the blocking system.

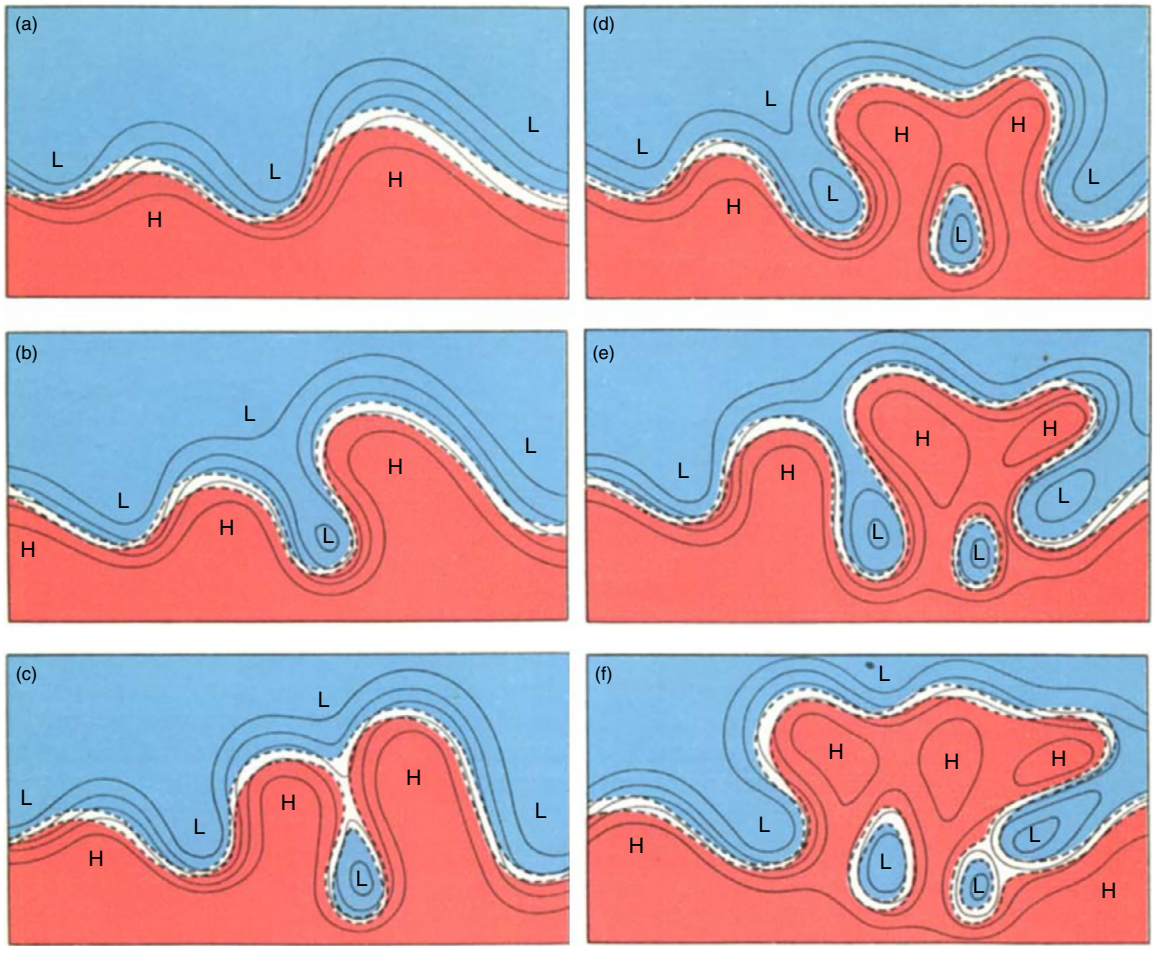

Fig. 21 Idealized development of an unstable wave to a blocking anticyclone. Warm air is shaded red, cold air is shaded blue and black lines show streamlines. Local maxima (H) and minima (L) in the geopotential height field and frontal boundaries (dashed lines) are also shown. Figure from Berggren R, Bolin B, and Rossby CG (1949) An aerological study of zonal motion, its perturbations and break-down. *Tellus* 1(2): 14–37.

Lifecycle of blocking

In recent decades, the mechanisms responsible for atmospheric blocking have been studied, elucidating key processes that are known to influence blocking dynamics. However, despite this progress, a complete blocking theory is still lacking (Woollings et al., 2018) due to their complexity. In addition, the contribution of various mechanisms towards blocking varies in both space and time, which further compounds the difficulty in obtaining a complete dynamical blocking framework.

In what follows, blocking mechanisms will be considered from a potential vorticity (PV) perspective (see Glossary). Atmospheric blocking is characterized by low PV (or negative PV anomalies), and therefore any process that modifies the PV within a block can be influential for its dynamics. This change in PV is achieved through:

i. A PV flux in or out of the block.
ii. Advection of PV in or out of the block.
iii. Local PV modification through frictional or diabatic processes.
iv. Any combination of (i)–(iii).

Some of the mechanisms responsible for various stages of the blocking lifecycle (onset, maintenance, and decay) are discussed, and the ways in which they alter the PV in a block are examined.

Block onset

Overturning within the large-scale planetary circulation (Fig. 22a–c); known as Rossby wave breaking, (RWB) is a common way in which low-PV (i.e., anticyclonic) air is brought polewards towards mid-latitudes. When this air becomes cut-off from the rest of the planetary flow pattern (Fig. 22d), a blocking pattern can become established (Masato et al., 2012). Wave-breaking is defined by the direction of overturning (i.e., anticyclonic or cyclonic), with both directions being responsible for blocking of various types. Cyclonic RWB is typically associated with more persistent blocking anticyclones, whereas shorter lived blocks preferentially result from anticyclonic wave breaking (Drouard et al., 2021).

Extratropical cyclones have also been shown to be important for the formation of blocking events. Rapid cyclogenesis produces both a large warm sector within the cyclone, and a strong ridge immediately downstream. Therefore, cyclones are not only responsible for pre-conditioning the atmosphere for blocking by promoting ridge development, but they can also assist in amplifying the ridge via the advection of subtropical air, with low PV, into the ridge via its warm conveyor belt (WCB). Additionally, negative PV anomalies generated within the cyclone itself are also routinely brought into the upper-level circulation of an incipient block which further promotes its development. Diabatic heating within the cyclone's WCB is responsible for the creation of upper-level negative PV anomalies, which are then advected into the block via the divergent upper-level outflow of the WCB. Almost half of the air within blocking anticyclones undergoes strong diabatic heating (median of 8.5 K) 3 days prior to entering a block, and diabatically driven blocks are known to be larger and stronger than non-diabatic blocks (Steinfeld and Pfahl, 2019).

Block maintenance

Once the PV structure of the block has been established, it must be maintained for a block to persist. The interaction of blocks with smaller, synoptic-scale eddies (ridges and troughs in the jet stream) has long been known to be an important mechanism through which blocks are maintained. There are two principal ways in which these eddies can influence blocking dynamics, which are summarized in Fig. 23 using a Rex block (see Fig. 21e) as a demonstration.

Firstly, as eddies of either polarity approach blocks, the splitting of the jet stream around the blocking pattern leads to those eddies being deformed and strained ($t = 0$–1 in Fig. 23). Shutts (1983) demonstrated that the dissipation of eddy energy immediately upstream of the block leads to an equatorward eddy vorticity (ζ') flux (black arrow in Fig. 23). The result of this is to decrease (make more anticyclonic) the PV on the poleward side of the split and increase it (make more cyclonic) on the equatorward side (Fig. 23 shading). Therefore, the Rex blocking pattern is reinforced due to the straining of synoptic cyclones and anticyclones upstream of the block.

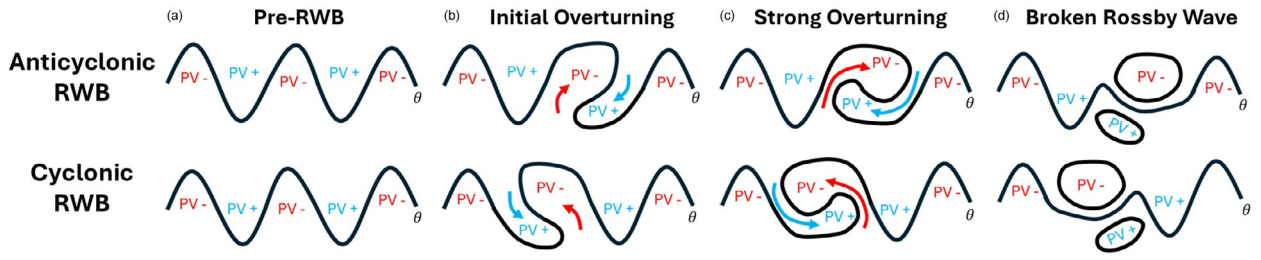

Fig. 22 Schematic showing the process of RWB in both an anticyclonic (top) and cyclonic (bottom) direction, in the Northern Hemisphere. The black line depicts an arbitrary isotherm on a constant PV surface, ridges and troughs are shown by "PV+" and "PV−," respectively. The arrows indicate the direction and amplitude of the wave overturning.

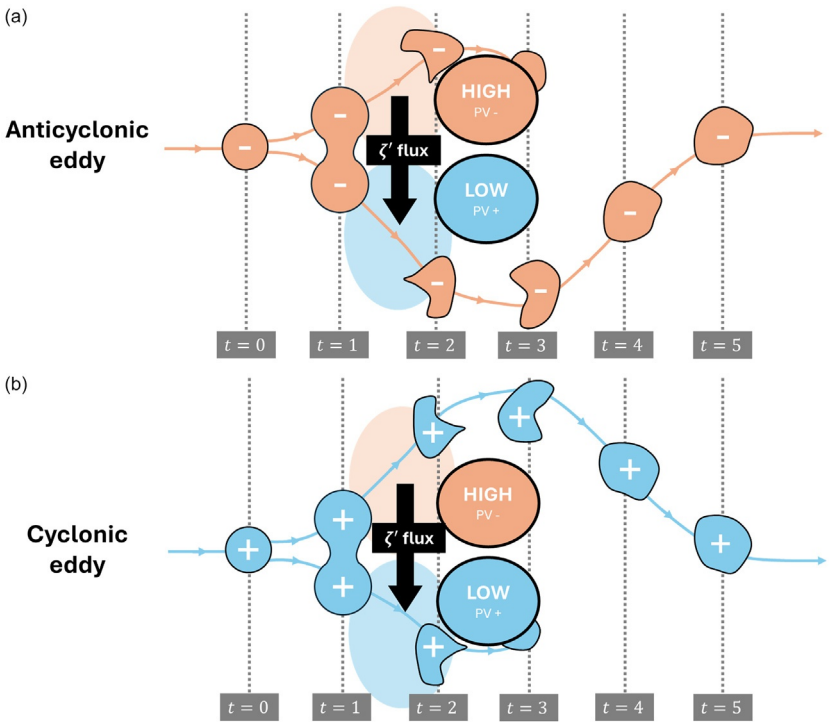

Fig. 23 Schematic of how synoptic eddies, in a background westerly flow, are strained and attracted by blocks. A dipole block is shown in the figure with the anticyclonic and cyclonic vortices labelled "HIGH" and "LOW," respectively. Anticyclonic eddies in (a) are denoted with a "PV−" in red shading, and cyclonic eddies in (b) are denoted with a "PV+" in blue shading. The eddy vorticity flux induced by eddy straining is shown by the black arrow, with the resultant (potential) vorticity forcing shown in pale red (anticyclonic) and blue (cyclonic). The red/blue arrows show the paths of the anticyclonic/cyclonic eddies when they are attracted or repelled by the block. The time stamps denoted by the "t" are arbitrary.

More recently, it has been demonstrated that synoptic eddies are not only strained around blocks but are also attracted and repelled by the block (red and blue arrows in Fig. 23), as discussed in Yamazaki and Itoh (2013). Unlike with eddy straining however, the polarity of the eddy is important for the attraction/repulsion towards/away from the block and therefore the direct PV tendency applied to each part of the block. When a synoptic anticyclone (Fig. 23a) passes to the north, it is attracted by the blocking high ($t = 2$) and ultimately absorbed into the blocking high's vortex ($t = 3$). On the other hand, when deflected to the south of the block, synoptic anticyclones are repelled by the blocking low and are not absorbed into the blocking system ($t = 2$–5). Therefore, the PV of blocking anticyclones can be thought of as being replenished by the mixing with synoptic-scale anticyclones. Indeed, the work by Suitters et al. (2023) has shown that there is a positive correlation between number of synoptic anticyclones absorbed by the blocking high and its persistence. Synoptic cyclones are conversely repelled by blocking anticyclones and absorbed by the cyclonic part of the block (Fig. 23b).

Diabatic processes can also modify the PV signature of blocking during its maintenance phase. For example, events known as "latent heat bursts" occur in extratropical cyclones, which lead to additional upper-level PV decreases once the block is already established. On average, atmospheric blocks receive negative PV input from 2 to 3 latent heat bursts throughout their lifetime (Steinfeld and Pfahl, 2019). Additionally, further RWB can also help to bring further low-PV air from the subtropics into the block and help maintain it.

Block decay

Less is understood about the mechanisms behind the decay of blocks, compared to their onset and maintenance. A simplistic way of understanding block decay is that it occurs once the maintenance processes of the block have ceased. Given an appropriate change in the planetary circulation pattern, blocks can be advected downstream and become transient features, which ends the blocking event at a particular location. Processes leading to a negative PV flux divergence (i.e., PV flux convergence), or sources of PV can also lead to block decay. Examples of the latter include frictional dissipation or atmospheric cooling via outgoing longwave radiation.

Block forecasting

Although blocking has been recognized for many decades, its accurate and timely prediction still presents a problem in medium-range numerical weather prediction (NWP). A particularly prominent issue is the accurate forecasting of the timing of block decay, with forecasts often under-predicting the period over which a block lasts (i.e., its persistence). One way of reducing the uncertainty and increasing the reliability of blocking forecasts is to utilize an ensemble of simulations. By using an ensemble of

forecasts, a range of plausible evolutions of the atmosphere are presented to a forecaster, and as a result a probabilistic forecast can be produced that gives the likelihood of a block occurring at a particular time and location. This approach is an area of ongoing research and is seen as more useful than a deterministic forecast, which gives only a single representation of the forecast atmospheric state.

Impacts and preferred locations

Atmospheric blocking plays a crucial role in shaping weather patterns, climate, and environmental conditions, particularly in mid-latitude regions. When blocking patterns persist, they can lead to extreme weather conditions, not only in the areas directly affected by the high-pressure system but also in regions located upstream and downstream of the block (Lupo, 2021; Kautz et al., 2022).

Atmospheric blocking is primarily associated with unusual temperature and precipitation patterns. Fig. 24 shows that the effects of blocking vary by season and depend on the sector of the block. In summer, the high pressure caused by atmospheric blocking clears the skies of clouds and advects warm air, often leading to extreme high temperatures (Fig. 24b). Significant heatwaves, such as the European heatwaves of 2003 and 2010, and the 2021 western North American heatwave, were linked to blocking events. As the heat persists, dry conditions can favor wildfires (Antokhina et al., 2023). Thunderstorms are common on the blocking system's eastern and western flanks. During winter, atmospheric blocking can bring cold air from the north, leading to cold spells, particularly downstream of the blocking system (Fig. 24a). An example is the North American cold wave of 2014 (Shi et al., 2017).

In addition to temperature extremes, persistent blocking can modify typical precipitation regimes, leading to hydrological extremes such as droughts. For example, blocking can deflect weather systems like winter storms away from certain regions, exacerbating water deficiency and leading to severe droughts. Notable cases include the Sao Paulo droughts of 2013–2015 (Seth et al., 2015). Moreover, blocking patterns can contribute to heavy rainfall in certain regions, resulting in flooding. A famous example are the 2010 Pakistan floods, which were associated with recurrent blocks over western Russia, favoring the presence of low-pressure systems downstream of the blocks (Martius et al., 2013), and are an example of how blocking can be associated with compounding impacts.

Not only do atmospheric blocking events vary considerably in how often and long they occur, but they also have preferential areas and times of year for formation, shown in Fig. 25. In both hemispheres, blocking occurrence is at a maximum in winter and a minimum in summer. For the Northern Hemisphere, intense blocking events are common in both summer and winter. Fig. 25 shows that during winter, they tend to occur more frequently in the Euro-Atlantic region and over the North Pacific. In summer, these events are more likely to occur in Eastern Europe and Western Russia. In contrast, since the Southern Hemisphere experiences stronger zonal (west-to-east) winds, blocking events are shorter-lived and less frequent compared to the Northern Hemisphere. However, Southern Hemisphere blocks still play an essential role for the same types of surface impacts as in the Northern

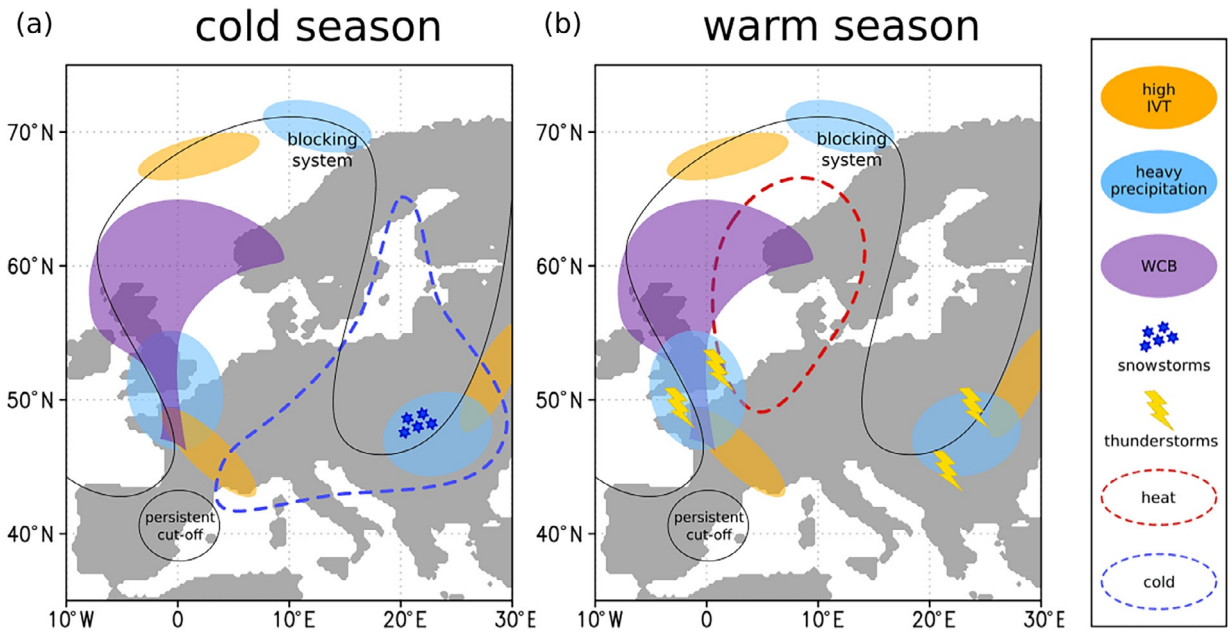

Fig. 24 Schematic showing an example of northern European blocking and its associated weather extremes in (a) winter and (b) summer. Map lines delineate study areas and do not necessarily depict accepted national boundaries. Figure from Kautz L-A, Martius O, Pfahl S, Pinto JG, Ramos AM, Sousa PM, and Woollings T (2022) Atmospheric blocking and weather extremes over the euro-Atlantic sector—A review. *Weather and Climate Dynamics* 3(1): 305–36. https://doi.org/10.5194/wcd-3-305-2022, https://wcd.copernicus.org/articles/3/305/2022/.

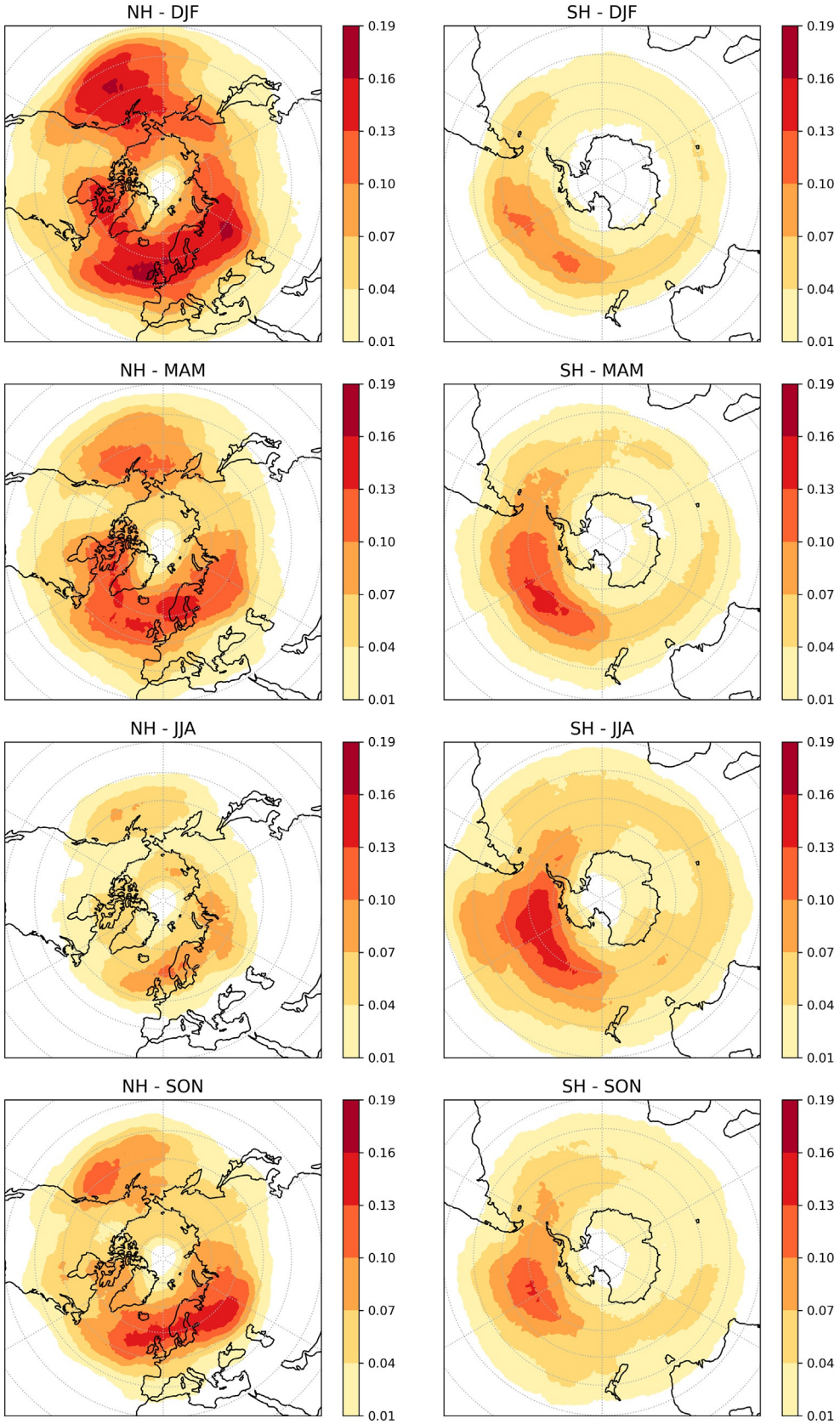

Fig. 25 Climatological blocking occurrence (fraction of days in a season that are blocked) for the Northern Hemisphere (NH, left) and Southern Hemisphere (SH, right) in December-January-February (DJF), March-April-May (MAM), June-July-August (JJA) and September-October-November (SON). Derived from 6-hourly ERA5 500 hPa geopotential height data (1940–2023) following the method of Suitters et al. (2023). Map lines delineate study areas and do not necessarily depict accepted national boundaries.

Hemisphere. Certain areas are more prone to blocking events in the Southern Hemisphere, including three main areas: New Zealand, the southern and southeastern Andes, and the southern Pacific Ocean. Intense blocking events in the Southern Hemisphere are more common in winter than summer.

Long-term climate impacts can result from feedback processes between atmospheric blocking and various climate system components. For example, prolonged heat waves or cold spells can influence the extent of sea ice, affecting atmospheric circulation patterns (Woollings et al., 2018). Blocking also plays a role in moisture transport towards Antarctica, which can impact the Antarctic ice sheet by producing snowfall, thereby influencing the continent's surface mass balance (Wille et al., 2021) and potentially affecting sea level rise. Similarly, moisture transport towards the Arctic, driven by blocking, plays a crucial role in the Northern Hemisphere ice sheet.

Blocking events directly affect various societal, economic, and ecological sectors. For instance, the 2003 European heatwave associated with blocking caused forest fires and severe droughts, leading to estimated losses of €13.1 billion (García-Herrera et al., 2010). Below, we describe the impacts of blocking on agriculture, the energy industry, health, and ecosystems:

- Agriculture: Blocking can severely disrupt agriculture by causing extreme temperatures, droughts, or excessive rainfall, which may lead to crop failures and food shortages. For example, during the February 2012 cold wave in Eastern Europe, temperatures dropped to nearly −30 °C, causing severe damage to Moldavia's vineyards (Planchon et al., 2015).
- Energy industry: Extended periods of extreme heat or cold associated with blocking can lead to sharp increases in energy demand, putting strain on energy infrastructure and reducing renewable energy production (Grams et al., 2017). During the 2003 European summer heatwave, mean electricity prices rose to nearly €100 MWh^{-1}, a significant increase from the approximately €40 MWh^{-1} observed the previous year (Fink et al., 2004).
- Health: Heatwaves and cold spells linked to blocking can trigger significant public health crises, including heat-related illnesses, respiratory issues, and increased mortality. In addition to temperature extremes, recent studies show that blocking contributes to poor air quality, including higher levels of ozone (Otero et al., 2022).
- Ecosystems: Prolonged blocking events can stress ecosystems, leading to shifts in species distributions, disruptions in migration patterns, and increased vulnerability to extreme weather. For instance, the 2003 European heatwave resulted in the loss of 5–10% of the total ice mass in Alpine glaciers (García-Herrera et al., 2010).

A recent major extreme weather event associated with blocking occurred in Europe during the summer of 2021 (described in the Cut-off lows section above). While several southeastern European and Baltic countries experienced extreme temperatures, devastating floods impacted Germany, France, and the Benelux region. The German floods caused 184 fatalities. One of the drivers of these events was recurrent atmospheric blocking and wave breaking (Tuel et al., 2022). Fig. 26 shows the anomaly in blocking frequency, highlighting an excess of blocking in Eastern Europe.

Given the significant impact of blocking, it is essential to implement adaptation measures to mitigate its effects. Strategies to reduce vulnerability to blocking-induced extreme weather include improving infrastructure resilience, enhancing water management, and developing action plans for heatwaves and cold spells. Climate policy plays a crucial role in this process. A better understanding of the effects of atmospheric blocking can guide policies for adapting to the increasing frequency of extreme weather events driven by climate change.

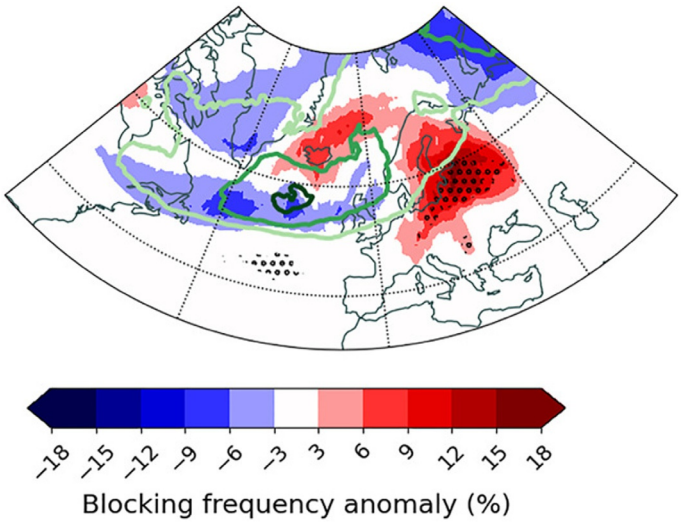

Fig. 26 Blocking frequency anomaly during 15 June-15 July 2021 (colors) and climatology (green contours at 5%, 7.5%, and 10%). Map lines delineate study areas and do not necessarily depict accepted national boundaries. From Tuel A, Steinfeld D, Ali SM, Sprenger M, and Martius O (2022) Large-scale drivers of persistent extreme weather during early summer 2021 in Europe. Geophysical Research Letters 49(18): e2022GL099624. https://doi.org/10.1029/2022GL099624.

Conclusion

It is clear from the text that weather features of the mid-latitudes are highly varied, complex and impactful on the daily lives of the populations who live in those regions. The complexity arises from the combination of unequal heating of the Earth's surface (warm equator, cold poles) and its rotation. Two primary types of large-scale circulatory system dominate the region—extratropical cyclones and blocking anticyclones.

Extratropical cyclones follow two main lifecycle sequences known as the "Norwegian" and "Shapiro-Keyser" models. Other cyclonic lifecycles do occur, for example continental cyclones in the lee of high topography (e.g., to the east of the Rocky Mountains); however, the Norwegian and Shapiro-Keyser models dominate and are frequently found over the mid-latitude ocean basins of both hemispheres. Extratropical cyclones also induce air flows that are responsible for most of the precipitation and hazardous winds within their extent. Extratropical cyclones are often accompanied by fronts too, which are associated with most of the precipitation in the mid-latitudes.

Conversely, anticyclones circulate in the opposite direction to extratropical cyclones and are characterized by high surface pressure, suppression of precipitation-bearing clouds and generally calm weather. Large anticyclones can block the normal progression of extratropical cyclones and are therefore known as "blocks." Once these blocks are in place they tend to be stationary (or very slow moving) and can therefore persist for several days to weeks by self-sustaining mechanisms. Block occurrence is more frequent in the winter than the summer for both hemispheres, which leads to either extreme cold (winter) conditions or very high temperatures and drought (summer). The extreme weather associated with blocking has large impacts on the agricultural, energy and health sectors as well as the ecosystem.

While this article has provided a comprehensive overview of the weather systems that affect the mid-latitudes with reference to many scientific articles, further information on the fundamental principles elucidated above can be found in: Ahrens (2000), Lackmann (2011), Martin (2006), and McIlveen (1992).

References

Ahmadi-Givi F, Graig GC, and Plant RS (2004) The dynamics of a midlatitude cyclone with very strong latent-heat release. *Quarterly Journal of the Royal Meteorological Society* 130(596): 295–323.

Ahrens DC (2000) *Meteorology Today An introduction to Weather, Climate, and the Environment*, sixth ed. Pacific Grove: Brooks/Cole.

Antokhina OY, Antokhin PN, Belan BD, Gochakov AV, Martynova YV, Pustovalov KN, Tarabukina LD, and Devyatova EV (2023) Effects of Rossby waves breaking and atmospheric blocking formation on the extreme forest fire and floods in eastern Siberia 2019. *Fire* 6(3): 122. https://doi.org/10.3390/fire6030122.

Berggren R, Bolin B, and Rossby CG (1949) An aerological study of zonal motion, its perturbations and break-down. *Tellus* 1(2): 14–37.

Bjerknes J (1919) On the structure of moving cyclones. *Geophysica Norvegica* 1(2): 1–8. https://geofysikk.org/NGF/GeoPub/NGF_GP_Vol01_no2.pdf.

Bjerknes J and Solberg H (1922) Life cycle of cyclones and the polar front theory of atmospheric circulation. *Geophysica Norvegica* 3(1): 3–18. https://geofysikk.org/NGF/GeoPub/NGF_GP_Vol03_no1.pdf.

Bozkurt D, Rondanelli R, Garreaud R, and Arriagada A (2016) Impact of Warmer Eastern tropical pacific SST on the March 2015 Atacama Floods. *Monthly Weather Review* 144: 4441–4460. https://doi.org/10.1175/MWR-D-16-0041.1.

Browning KA (1990) Organization of clouds and precipitation in extratropical cyclones. In: Newton CW and Holopainen EO (eds.) *Extratropical Cyclones, The Erik Palmén Memorial Volume*, pp. 129–153. Boston: American Meteorological Society. https://doi.org/10.1007/978-1-944970-33-8_8.

Browning KA (1997) The dry intrusion perspective of extra-tropical cyclone development. *Meteorological Applications* 4(4): 317–324.

Browning KA (2004) The sting at the end of the tail: Damaging winds associated with extratropical cyclones. *Quarterly Journal of the Royal Meteorological Society* 130(597): 375–399. https://doi.org/10.1256/qj.02.143.

Browning KA and Golding BW (1995) Mesoscale aspects of a dry intrusion within a vigorous cyclone. *Quarterly Journal of the Royal Meteorological Society* 121(523): 463–493.

Browning KA and Wang C-G (2002) Cloud-top striations above ana-cold frontal circulations. *Quarterly Journal of the Royal Meteorological Society* 128(580): 477–489. https://doi.org/10.1256/003590002321042063.

Browning KA, Smart DJ, Clark MR, and Illingworth AJ (2015) The role of evaporating showers in the transfer of sting-jet momentum to the surface. *Quarterly Journal of the Royal Meteorological Society* 141(693): 2956–2971.

Burt SD and Mansfield DA (1988) The great storm of 15–16 October 1987. *Weather* 43(3): 90–110.

Carlson TN (1980) Airflow through midlatitude cyclones and the comma cloud pattern. *Monthly Weather Review* 108(10): 1498–1509.

Catto JL and Raveh-Rubin S (2019) Climatology and dynamics of the link between dry intrusions and cold fronts during winter. Part I. Global climatology. *Climate Dynamics* 53: 1873–1892. https://doi.org/10.1007/s00382-019-04745-w.

Catto JL, Jakob C, Berry G, and Nicholls N (2012) Relating global precipitation to atmospheric fronts. *Geophysical Research Letters* 39: L10805. https://doi.org/10.1029/2012GL051736.

Clark PA and Gray SL (2018) Sting jets in extratropical cyclones: A review. *Quarterly Journal of the Royal Meteorological Society* 144(713): 943–969.

Cusack S (2023) A long record of European windstorm losses and its comparison to standard climate indices. *Natural Hazards and Earth System Sciences* 23: 2841–2856. https://doi.org/10.5194/nhess-23-2841-2023.

Dacre HF, Clark PA, Martínez-Alvarado O, Stringer MA, and Lavers DA (2015) How do atmospheric rivers form? *Bulletin of the American Meteorological Society* 96(8): 1243–1255.

Drouard M, Woollings T, Sexton DM, and McSweeney CF (2021) Dynamical differences between short and long blocks in the Northern Hemisphere. *Journal of Geophysical Research-Atmospheres* 126(10): e2020JD034082.

Fink AH, Brücher T, Krüger A, Leckebusch GC, Pinto JG, and Ulbrich U (2004) The 2003 European summer heatwaves and drought-synoptic diagnosis and impacts. *Weather* 59(8): 209–216.

Fluck E and Raveh-Rubin S (2023) Dry air intrusions link Rossby wave breaking to large-scale dust storms in Northwest Africa: Four extreme cases. *Atmospheric Research* 286(106): 663.

García-Herrera R, Díaz J, Trigo RM, Luterbacher J, and Fischer EM (2010) A review of the European summer heat wave of 2003. *Critical Reviews in Environmental Science and Technology* 40(4): 267–306.

Gimeno L, Nieto R, Vázquez M, and Lavers DA (2014) Atmospheric rivers: A mini-review. *Frontiers in Earth Science* 2: 2. https://doi.org/10.3389/feart.2014.00002.

Givon Y, Keller D Jr, Pennel R, Drobinski P, and Raveh-Rubin S (2024) Decomposing the role of dry intrusions for ocean evaporation during mistral. *Quarterly Journal of the Royal Meteorological Society* 150(760): 1791–1808.
Grams C, Beerli R, Pfenninger R, Staffell I, and Wernli H (2017) Balancing Europe's wind-power output through spatial deployment informed by weather regimes. *Nature Climate Change* 7: 557–562.
Hersbach H, Bell B, Berrisford P, Biavati G, Horányi A, Muñoz Sabater J, Nicolas J, Peubey C, Radu R, Rozum I, Schepers D, Simmons A, Soci C, Dee D, and Thépaut J-N (2023) *ERA5 Monthly Averaged Data on Pressure Levels From 1940 to Present*. Copernicus Climate Change Service (C3S) Climate Data Store (CDS). https://doi.org/10.24381/cds.6860a573. https://cds.climate.copernicus.eu/datasets/reanalysis-era5-pressure-levels-monthly-means?tab=overview. (Accessed 21 October 2024).
Hewson TD and Neu U (2015) Cyclones, windstorms and the IMILAST project. *Tellus A* 67(1): 27,128.
Hirata H, Kawamura R, Nonaka M, and Tsuboki K (2019) Significant impact of heat supply from the Gulf Stream on a "superbomb" cyclone in January 2018. *Geophysical Research Letters* 46: 7718–7725. https://doi.org/10.1029/2019GL082995.
Hobbs PV, Locatelli JD, and Martin JE (1996) A new conceptual model for cyclones generated in the Lee of the Rocky Mountains. *Bulletin of the American Meteorological Society* 77: 1169–1178. https://doi.org/10.1175/1520-0477(1996)077<1169:ANCMFC>2.0.CO;2.
Hoskins BJ (1975) The geostrophic momentum approximation and the semi-geostrophic equations. *Journal of the Atmospheric Sciences* 32: 233–242. https://doi.org/10.1175/1520-0469(1975)032<0233:TGMAAT>2.0.CO;2.
Hoskins BJ and Hodges KI (2019) The annual cycle of northern hemisphere storm tracks. Part I. Seasons. *Journal of Climate* 32: 1743–1760. https://doi.org/10.1175/JCLI-D-17-0870.1.
Ilotoviz E, Ghate VP, and Raveh-Rubin S (2021) The impact of slantwise descending dry intrusions on the marine boundary layer and air-sea interface over the ARM Eastern North Atlantic site. *Journal of Geophysical Research-Atmospheres* 126: e2020JD033879. https://doi.org/10.1029/2020JD033879.
Joos H and Wernli H (2012) Influence of microphysical processes on the potential vorticity development in a warm conveyor belt: A case-study with the limited-area model COSMO. *Quarterly Journal of the Royal Meteorological Society* 138: 407–418. https://doi.org/10.1002/qj.934.
Kautz L-A, Martius O, Pfahl S, Pinto JG, Ramos AM, Sousa PM, and Woollings T (2022) Atmospheric blocking and weather extremes over the euro-Atlantic sector—A review. *Weather and Climate Dynamics* 3(1): 305–336. https://doi.org/10.5194/wcd-3-305-2022, https://wcd.copernicus.org/articles/3/305/2022/.
Keyser D (1999) On the representation and diagnosis of frontal circulations in two and three dimensions. In: Shapiro MA and Grønås S (eds.) *The Life Cycles of Extratropical Cyclones*, pp. 239–264. American Meteorological Society. https://doi.org/10.1007/978-1-935704-09-6_17.
Klaider N and Raveh-Rubin S (2023) Extended influence of midlatitude cyclones on global cold extremes. *Geophysical Research Letters* 50(20): e2023GL104999.
Lackmann G (2011) *Midlatitude Synoptic Meteorology Dynamics, Analysis and Forecasting*. Boston: American Meteorological Society.
Lim EP and Simmonds I (2002) Explosive cyclone development in the Southern Hemisphere and a comparison with Northern Hemisphere events. *Monthly Weather Review* 130(9): 2188–2209.
Lupo AR (2021) Atmospheric blocking events: a review. *Annals New York Academy of Sciences* 1504(1): 5–24. https://doi.org/10.1111/nyas.14557.
Madonna E, Wernli H, Joos H, and Martius O (2014) Warm conveyor belts in the ERA-Interim dataset (1979–2010). Part I. Climatology and potential vorticity evolution. *Journal of Climate* 27(1): 3–26.
Magaritz-Ronen L and Raveh-Rubin S (2023) Tracing the formation of exceptional fronts driving historical fires in Southeast Australia. *npj Climate and Atmospheric Science* 6(1): 110.
Martin JE (1999) Quasigeostrophic forcing of ascent in the occluded sector of cyclones and the Trowal airstream. *Monthly Weather Review* 127: 70–88. https://doi.org/10.1175/1520-0493(1999)127<0070:QFOAIT>2.0.CO;2.
Martin JE (2006) *Mid-Latitude Atmospheric Dynamics A First Course*. Chichester: John Wiley and Sons.
Martínez-Alvarado O, Baker LH, Gray SL, Methven J, and Plant RS (2014) Distinguishing the cold conveyor belt and sting jet airstreams in an intense extratropical cyclone. *Monthly Weather Review* 142(8): 2571–2595.
Martius O, Sodemann H, Joos H, Pfahl S, Winschall A, Croci-Maspoli M, Graf M, Madonna E, Mueller B, Schemm S, Sedláček J, Sprenger M, and Wernli H (2013) The role of upper-level dynamics and surface processes for the Pakistan flood of July 2010. *Quarterly Journal of the Royal Meteorological Society* 139(676): 1780–1797. https://doi.org/10.1002/qj.2082.
Masato G, Hoskins B, and Woollings TJ (2012) Wave-breaking characteristics of midlatitude blocking. *Quarterly Journal of the Royal Meteorological Society* 138(666): 1285–1296.
McIlveen R (1992) *Fundamentals of Weather and Climate*. Cheltenham: Stanley Thornes (Publishers) Ltd.
Mohr S, Ehret U, Kunz M, Ludwig P, Caldas-Alvarez A, Daniell JE, Ehmele F, Feldmann H, Franca MJ, Gattke C, Hundhausen M, Knippertz P, Küpfer K, Mühr B, Pinto JG, Quinting J, Schäfer AM, Scheibel M, Seidel F, and Wisotzky C (2023) A multi-disciplinary analysis of the exceptional flood event of July 2021 in central Europe. Part 1. Event description and analysis. *Natural Hazards and Earth System Sciences* 23: 525–551. https://doi.org/10.5194/nhess-23-525-2023.
Muñoz C, Schultz D, and Vaughan G (2020) A midlatitude climatology and interannual variability of 200- and 500-hPa cut-off lows. *Journal of Climate* 33: 2201–2222. https://doi.org/10.1175/JCLI-D-19-0497.1.
Otero N, Jurado OE, Butler T, and Rust HW (2022) The impact of atmospheric blocking on the compounding effect of ozone pollution and temperature: A copula-based approach. *Atmospheric Chemistry and Physics* 22(3): 1905–1919. https://doi.org/10.5194/acp-22-1905-2022.
PERILS (2024) *PERILS Final Industry Loss Estimates for Windstorm Ciarán*. https://www.perils.org/news/eur-2-067m-perils-releases-final-industry-loss-estimate-for-windstorm-ciaran-of-november-2023.
Pinheiro H, Gan M, and Hodges K (2021) Structure and evolution of intense austral cut-off lows. *Quarterly Journal of the Royal Meteorological Society* 147: 1–20. https://doi.org/10.1002/qj.3900.
Planchon O, Quénol H, Irimia L, and Patriche C (2015) European cold wave during February 2012 and impacts in wine growing regions of Moldavia (Romania). *Theoretical and Applied Climatology* 120: 469–478.
Priestley MD, Ackerley D, Catto JL, Hodges KI, McDonald RE, and Lee RW (2020) An overview of the extratropical storm tracks in CMIP6 historical simulations. *Journal of Climate* 33(15): 6315–6343.
Raveh-Rubin S (2017) Dry intrusions: Lagrangian climatology and dynamical impact on the planetary boundary layer. *Journal of Climate* 30(17): 6661–6682.
Raveh-Rubin S and Wernli H (2016) Large-scale wind and precipitation extremes in the Mediterranean: dynamical aspects of five selected cyclone events. *Quarterly Journal of the Royal Meteorological Society* 142: 3097–3114. https://doi.org/10.1002/qj.2891.
Reed RJ, Albright MD, Sammons AJ, and Undén P (1988) The role of latent heat release in explosive cyclogenesis: Three examples based on ECMWF operational forecasts. *Weather Forecasting* 3: 217–229. https://doi.org/10.1175/1520-0434(1988)003<0217:TROLHR>2.0.CO;2.
Rex DF (1950) Blocking action in the middle troposphere and its effect upon regional climate. *Tellus* 2(4): 275–301.
Sanders F and Gyakum JR (1980) Synoptic-dynamic climatology of the "bomb". *Monthly Weather Review* 108(10): 1589–1606.
Schär C (2003) Lee cyclogenesis. In: Holton JR, Curry JA, and Pyle JA (eds.) *Encyclopedia of Atmospheric Sciences*, pp. 1602–1614. Academic Press, Elsevier Science Ltd.
Schemm S, Sprenger M, and Wernli H (2018) When during their life cycle are extratropical cyclones attended by fronts? *Bulletin of the American Meteorological Society* 99: 149–165. https://doi.org/10.1175/BAMS-D-16-0261.1.
Schultz DM (2001) Reexamining the cold conveyor belt. *Monthly Weather Review* 129(9): 2205–2225.
Schultz DM and Vaughan G (2011) Occluded fronts and the occlusion process: A fresh look at conventional wisdom. *Bulletin of the American Meteorological Society* 92: 443–466. https://doi.org/10.1175/2010BAMS3057.1.
Schultz DM and Zhang F (2007) Baroclinic development within zonally-varying flows. *Quarterly Journal of the Royal Meteorological Society* 133: 1101–1112. https://doi.org/10.1002/qj.87.

Seth A, Fernandes K, and Camargo SJ (2015) Two summers of São Paulo drought: Origins in the western tropical pacific. *Geophysical Research Letters* 42(24): 10816–10823. https://doi.org/10.1002/2015GL066314.

Shapiro MA and Keyser D (1990) Fronts, jet streams and the tropopause. In: Newton CW and Holopainen EO (eds.) *Extratropical Cyclones, The Erik Palmén Memorial Volume*, pp. 167–191. American Meteorological Society.

Shapiro MA, Wernli H, Bao J-W, Methven J, Xiaolei Z, Doyle J, Holt T, Donall-Grell E, and Neiman P (1999) A planetary-scale to mesoscale perspective of the life cycles of extratropical cyclones: The bridge between theory and observations. In: Shapiro MA and Grønås S (eds.) *The Life Cycles of Extratropical Cyclones*, pp. 139–185. American Meteorological Society. https://doi.org/10.1007/978-1-935704-09-6_14.

Shi C, Xu T, Li H, and Gao Y (2017) The role of Rossby-wave propagation in a North American extreme cold event. *Advances in Meteorology* 1: 4635849. https://doi.org/10.1155/2017/4635849.

Shutts G (1983) The propagation of eddies in diffluent jetstreams: Eddy vorticity forcing of 'blocking' flow fields. *Quarterly Journal of the Royal Meteorological Society* 109(462): 737–761.

Sousa PM, Barriopedro D, García-Herrera R, Woollings T, and Trigo RM (2021) A new combined detection algorithm for blocking and subtropical ridges. *Journal of Climate* 34: 7735–7758. https://doi.org/10.1175/JCLI-D-20-0658.1.

Steinfeld D and Pfahl S (2019) The role of latent heating in atmospheric blocking dynamics: A global climatology. *Climate Dynamics* 53(9): 6159–6180.

Suitters CC, Martínez-Alvarado O, Hodges KI, Schiemann RK, and Ackerley D (2023) Transient anticyclonic eddies and their relationship to atmospheric block persistence. *Weather and Climate Dynamics* 4(3): 683–700.

Thorncroft CD, Hoskins BJ, and McIntyre ME (1993) Two paradigms of baroclinic-wave life-cycle behaviour. *Quarterly Journal of the Royal Meteorological Society* 119: 17–55. https://doi.org/10.1002/qj.49711950903.

Tuel A, Steinfeld D, Ali SM, Sprenger M, and Martius O (2022) Large-scale drivers of persistent extreme weather during early summer 2021 in Europe. *Geophysical Research Letters* 49(18): e2022GL099624. https://doi.org/10.1029/2022GL099624.

Wernli H (1997) A Lagrangian-based analysis of extratropical cyclones. II. A detailed case-study. *Quarterly Journal of the Royal Meteorological Society* 123(542): 1677–1706.

Wille JD, Favier V, Gorodetskaya IV, Agosta C, Kittel C, Beeman JC, Jourdain NC, Lenaerts JTM, and Codron F (2021) Antarctic atmospheric river climatology and precipitation impacts. *Journal of Geophysical Research-Atmospheres* 126(8): e2020JD033788. https://doi.org/10.1029/2020JD033788.

Woollings T, Barriopedro D, Methven J, Son S-W, Martius O, Harvey B, Sillmann J, Lupo AR, and Seneviratne S (2018) Blocking and its response to climate change. *Current Climate Change Reports* 4: 287–300.

Yamazaki A and Itoh H (2013) Vortex–vortex interactions for the maintenance of blocking. Part I. The selective absorption mechanism and a case study. *Journal of the Atmospheric Sciences* 70(3): 725–742.

Young MV, Monk GA, and Browning KA (1987) Interpretation of satellite imagery of a rapidly deepening cyclone. *Quarterly Journal of the Royal Meteorological Society* 113(478): 1089–1115.